Jpn. J. Appl. Phys. Vol. 34 (1995) pp. 1–19
Part 1, No. 1, January 1995

Spin Dynamics Study in Conducting Polymers by Magnetic Resonance*1

Kenji MIZOGUCHI*2
Department of Physics, Tokyo Metropolitan University, Hachioji, Tokyo 192-03, Japan

(Received September 16, 1994; accepted for publication November 19, 1994)

We have applied the spin dynamics technique to conducting polymers, in particular, with the ESR method, and investigated microscopic transport properties in a quasi-one-dimensional (Q1D) polymer chain. This technique is a unique method for obtaining microscopic information on intrinsic transport properties, because macroscopic resistivity is mainly limited by electrical properties of interfacial regions between microcrystals. In this article, the principles and applications of this method will be reviewed in detail. The difference between ESR applied here and ^{1}H NMR will also be discussed, and each characteristic feature will be stressed.

KEYWORDS: conducting polymer, spin dynamics, ESR, NMR, linewidth, diffusion rate, electrical conductivity, relaxation time, frequency dependence, neutral soliton

1. Introduction

A vast number of investigations have been reported on the conducting polymers from not only fundamental but also practical aspects because of their novel properties: *e.g.*, new types of elementary excitations such as solitons and polarons, high conductivity, high anisotropy, flexibility, light weight, and large surface area[1,2] These conducting polymers doped heavily with acceptors or donors show typical metallic behavior, for example, Pauli susceptibility and thermoelectric power proportional to the temperature. Although electrical resistivity is another important property in investigating the conduction mechanism in the conducting polymers, it is well known to show semiconducting temperature dependence, which can be simulated by fluctuation-induced tunneling (Sheng's model)[3] or variable range hopping mechanisms.[4] This experimental finding has been interpreted to mean that the metallic regions are separated into many islands by semiconducting regions such as lightly doped regions, amorphous regions or interfibril regions. Some efforts were made to avoid this difficulty by analyzing the resistivity measured by the conventional four-terminal technique[5,6] and by a somewhat tricky voltage-shorted compaction (VSC) technique.[7] Here we report another microscopic technique to obtain information on the intrinsic transport properties: spin dynamics.

In this article, this distinctive technique on the dynamics of the spin carrier will be reviewed, especially by means of the frequency dependence of ESR.[8–20] Historically, the spin-lattice relaxation time T_1 in ^{1}H NMR instead of ESR has been used to study the spin dynamics in many kinds of organic charge transfer compounds and polymers.[21–25] In the heavily doped polyacetylene systems, however, we recently encountered a difficulty in studying the spin dynamics by means of ^{1}H NMR T_1 because large and non-metallic contribution rather than that of metallic electrons was observed, especially in the low-temperature region.[26,27]

Since spin carriers also have charge in many conducting polymers, the spin dynamics provides very interesting insights on microscopic electronic conduction in metallic regions. A conventional four-terminal measurement cannot provide sufficient information as to how the electrical conductivity behaves on or across the polymer chains. Therefore, results obtained by the spin dynamics technique are useful for discussing the mechanism of anisotropic and high electrical conductivity in the conducting polymers. Recent results on conductive polyaniline, polythiophene and poly(3-methylthiophene), and heavily doped polyacetylene will be discussed.

This review is organized as follows.

1. Introduction
2. Principles of Spin Dynamics
2.1 *Relaxation mechanism by diffusion motion of spins*
2.2 *Autocorrelation function and its spectral density*
2.3 *Spectral density in quasi-one-dimension*
2.3.1 *Spectral density*
2.3.2 *Effect of delocalized wave function*
2.4 *Spin-lattice T_1^{-1} and spin-spin T_2^{-1} relaxation rates*
2.5 *Effect of finite chain length*
3. Experimental
4. Neutral Soliton Dynamics in Pristine Trans-Polyacetylene
4.1 *ESR T_1^{-1} and T_2^{-1} (linewidth)*
4.2 *Effect of trapping*
4.2.1 *Diffuse/trap model*
4.2.2 *Anisotropy of ESR T_1^{-1} and linewidth*
4.2.3 *Anomalous broadening below 6 MHz in t-$(CH)_x$*
4.3 *Temperature dependence of diffusion rates*
4.4 *Relation to pulse ESR experiments*
4.4.1 *Spin-echo decay time T_M*
4.4.2 *Spin-lattice relaxation time*
4.4.3 *Multiple-quantum spin coherence*
5. Doped Polymers
5.1 *Polyaniline*
5.1.1 *Polyaniline*
5.1.2 *Protonation dependence of diffusion rate*
5.1.3 *Temperature dependence of diffusion rate*
5.2 *Polythiophene, poly(3-methylthiophene)*

*1This is revised, updated and translated version of the original paper which appeared in Oyo Buturi **60** (1991) 997 [in Japanese].

*2E-mail address: PXT00036@niftyserve.or.jp

5.2.1 *Materials*
5.2.2 *Frequency dependence of ESR linewidth*
5.2.3 *Temperature dependence of ESR linewidth*
5.2.4 *Parameters for electronic states*
5.3 *Polyacetylene*
5.3.1 *^{1}H NMR study of heavily doped polyacetylene*
5.3.2 *Temperature dependence of microscopic conductivity*
6. Comparison of ESR with NMR in Spin Dynamics Study
7. Concluding Remarks

2. Principles of Spin Dynamics

2.1 *Relaxation mechanism by diffusive motion of spins*

Electron spins with diffusive motion provide a characteristic relaxation mechanism for the nuclear and electron spin systems, especially in materials with low-dimensional electronic structures. A schematic description of this relaxation mechanism is given as follows.

As shown in Fig. 1(a), a radio-frequency (rf) coil containing a sample is set perpendicular to the external static magnetic field H_0. When the resonance condition $\omega_0=\gamma_s H_0$ is satisfied, spins are flipped from parallel to antiparallel with respect to H_0, absorbing an energy of $\hbar\omega_0$ from the rf oscillating magnetic field $H_1\cos(\omega_0 t)$. Here, $\hbar$ is Plank's constant divided by 2π and γ_s is the gyromagnetic ratio. The resulting excess population of the antiparallel spins relaxes to the thermal equilibrium value by releasing energy $\hbar\omega_0$ through spin-lattice interactions. The hyperfine interaction between electron and nuclear spins and the magnetic dipolar interaction between electron spins act as the spin-lattice interactions when they are modulated by the diffusive motion of the spins. The ω_0 component of the local fluctuating magnetic field H_{loc} at each spin site induces spin-flips.

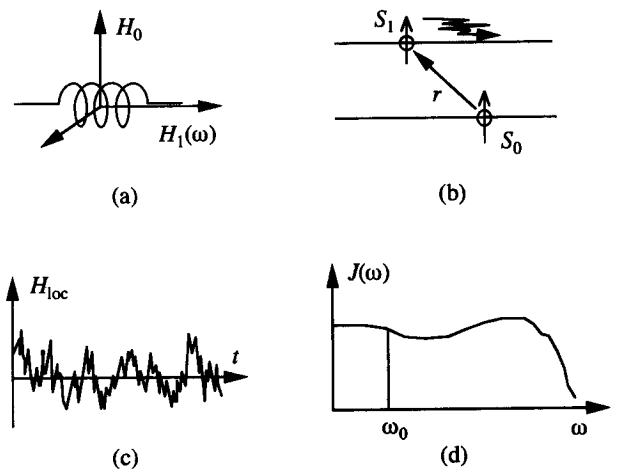

Fig. 1. Schematic explanation of the relaxation phenomena induced by the motion of spin. (a) Setting of the rf coil and the static magnetic field H_0 for magnetic resonance. (b) The relationship between two spins diffusing on the one-dimensional chains. (c) The local magnetic field modulated randomly by the spin motion, seen by the spin of interest as a function of the time. (d) The spectral density of the autocorrelation function of the local fluctuating magnetic field shown in (c).

Then, the excess population can relax to the thermal equilibrium state with a rate proportional to the spectral density $J(\omega_0)$ which is the Fourier transform of the autocorrelation function $G(t)$ for H_{loc}.

The hyperfine interaction is relatively important in the case of the neutral soliton in pristine *trans*-$(CH)_x$ because of its low spin concentration. In the conducting states, however, the dipolar interaction plays a dominant role because of its spin concentration which is higher by one or two orders of magnitude than in the case of the neutral soliton.

2.2 *Autocorrelation function and its spectral density*

An expression for the autocorrelation function $G(t)$ is given by Abragam[28] as

$$G(t)=\iint p(\boldsymbol{r}_1)\Phi(\boldsymbol{r}_1,\boldsymbol{r}_2,t)F(\boldsymbol{r}_1)F^*(\boldsymbol{r}_2)\,d\boldsymbol{r}_1\,d\boldsymbol{r}_2, \quad (2.1)$$

where $p(\boldsymbol{r}_1)$ is the probability density of finding a spin at $\boldsymbol{r}_1$, that is, the spin concentration c per unit molecule, $\Phi(\boldsymbol{r}_1,\boldsymbol{r}_2,t)$ is the probability density for the spin at $\boldsymbol{r}_1$ and $t=0$ to be found at $\boldsymbol{r}_2$ and time t, which is governed by the dimensionality of spin motion as will be discussed in §2.3. $F(\boldsymbol{r})$ is the random function of the implicit parameter t, which is determined by the functional form of the interaction Hamiltonian $\mathcal{H}_1=\Sigma_q F^{(q)}A^{(q)}$, for example, in the case of the dipolar interaction,

$$A^{(0)}=-\frac{3}{2}\gamma_I\gamma_S\hbar\left\{-\frac{2}{3}I_zS_z+\frac{1}{6}(I_+S_-+I_-S_+)\right\},$$
$$F^{(0)}=\frac{1-3\cos^2\theta}{r^3}, \quad (2.2.a)$$

$$A^{(\pm1)}=-\frac{3}{2}\gamma_I\gamma_S\hbar\{I_zS_\pm+I_\pm S_z\},$$
$$F^{(\pm1)}=\frac{\sin\theta\cos\theta\,e^{\mp i\varphi}}{r^3}, \quad (2.2.b)$$

$$A^{(\pm2)}=-\frac{3}{4}\gamma_I\gamma_S\hbar I_\pm S_\pm,$$
$$F^{(\pm2)}=\frac{\sin^2\theta\,e^{\mp2i\varphi}}{r^3}, \quad (2.2.c)$$

represented in polar coordinates with respect to H_0, where r is the length of the vector $\boldsymbol{r}$ connecting two spins.

Since the chains consist of discrete atoms or molecules in the actual systems, we redefine $G(t)$ as

$$G^{(j)}(t)=c\sum_{\boldsymbol{r}_1,\boldsymbol{r}_2}\Phi(\boldsymbol{r}_1,\boldsymbol{r}_2,t)F^{(j)}(\boldsymbol{r}_1)F^{(j)*}(\boldsymbol{r}_2). \quad (2.3)$$

The Fourier transform of $G(t)$ then gives the spectral density $J(\omega)$ as

$$J^{(j)}(\omega)=c\sum_{\boldsymbol{r}_1,\boldsymbol{r}_2}\phi(\boldsymbol{r}_1,\boldsymbol{r}_2,\omega)F^{(j)}(\boldsymbol{r}_1)F^{(j)*}(\boldsymbol{r}_2), \quad (2.4)$$

where $\phi(\boldsymbol{r}_1,\boldsymbol{r}_2,\omega)$ is the Fourier transform of the probability density $\Phi(\boldsymbol{r}_1,\boldsymbol{r}_2,t)$ and the sum is over $\boldsymbol{r}_1$ and $\boldsymbol{r}_2$ with all the possible sites.

2.3 *Spectral density in quasi-one dimension*

2.3.1 *Spectral density*

If we consider the spins diffusing on a one-dimensional (1D) chain with a diffusion coefficient $\mathcal{D}_{/\!/}$ (cm^2/s) or a diffusion rate $D_{/\!/}$ (rad/s)($=\mathcal{D}_{/\!/}/c_{/\!/}^2$; $c_{/\!/}$ is the lattice constant), the probability density $\Phi_{1D}(\boldsymbol{r}_1, \boldsymbol{r}_2, t)$ is given by a solution of the 1D diffusion equation, $\partial\Phi/\partial t = \mathcal{D}_{/\!/}\Delta\Phi$ which is valid in a longer time scale than $1/D_{/\!/}$. It is well known that the solution of this equation is given by

$$\Phi_{1D}(r_1, r_2, t)=\frac{1}{\sqrt{4\pi D_{/\!/}t}}\exp\left\{-\frac{(|r_1-r_2|/c_{/\!/})^2}{4D_{/\!/}t}\right\}. \quad (2.5)$$

Here, note that $D_{/\!/}$ should be replaced by $2D_{/\!/}$ for the electron-electron dipolar case in which the spins diffuse mutually. Since the actual systems are more or less quasi-one-dimensional (Q1D), we must take account of a cutoff of the 1D correlation of motion as the escape probability from the 1D-chain by adopting $\Phi_\perp(t)=\exp(-2t/\tau_\perp)$, where $\tau_\perp$ is the mean lifetime of the 1D correlation. If we consider the interesting case of Q1D diffusion, we have $D_\perp=1/\tau_\perp$. The probability density for the Q1D system can then be given by

$$\Phi_{Q1D}(r_1, r_2, t)=\Phi_{1D}(r_1, r_2, t)\cdot\Phi_\perp(t) =\frac{\exp\{-2D_\perp t\}}{\sqrt{4\pi D_{/\!/}t}}\exp\left\{-\frac{(|r_1-r_2|/c_{/\!/})^2}{4D_{/\!/}t}\right\}. \quad (2.6)$$

The expected frequency dependence of the spectral density $J(\omega)$ for the quasi-one-dimensional diffusion is given by the Fourier transform of eq. (2.6):

$$\phi_{Q1D}(|r_1-r_2|, \omega)=\frac{1}{\sqrt{4D_{/\!/}D_\perp}}\sqrt{\frac{1+\sqrt{1+(\omega/2D_\perp)^2}}{1+(\omega/2D_\perp)^2}} \times\exp(-\eta u)\left[\cos(\eta v)-\frac{v}{u}\sin(\eta v)\right], \quad (2.7)$$

where

$$\eta=\frac{|r_1-r_2|}{c_{/\!/}}\sqrt{\frac{2D_\perp}{D_{/\!/}}}, \quad u=\sqrt{\frac{\sqrt{1+(\omega/2D_\perp)^2}+1}{2}},$$

and

$$v=\sqrt{\frac{\sqrt{1+(\omega/2D_\perp)^2}-1}{2}}.$$

Although eq. (2.7) is complicated, we have a simplified formula,

$$\phi_{Q1D}(\omega)\approx\frac{1}{\sqrt{4D_{/\!/}D_\perp}}\sqrt{\frac{1+\sqrt{1+(\omega/2D_\perp)^2}}{1+(\omega/2D_\perp)^2}}, \quad (2.8)$$

for the scalar interaction ($\propto\delta(r_1-r_2)$) and the dipolar interaction under the condition $\eta u\ll 1$, i.e., $\omega\ll D_{/\!/}c_{/\!/}^2/\Delta r_{eff}^2$, where Δr_{eff} is the effective range of interaction. Actually, Δr_{eff} falls within several angstrom in which the dipolar coupling strength reduces to several % of its maximum value by virtue of the $1/(r_1^3 r_2^3)$ dependence, as shown by eqs. (2.1) and (2.2). Therefore, $\eta u\ll 1$ approximately holds at all the frequencies $\omega\ll D_{/\!/}$ where the diffusion equation is valid.

Then the spectral density $J(\omega)$ can be described by eq. (2.8) and the two simplified expressions are valid in each frequency regime:

$$\phi_{Q1D}(\omega)\approx\frac{1}{\sqrt{2D_{/\!/}\omega}}, \quad \text{for} \quad D_\perp\ll\omega\ll D_{/\!/}, \quad (2.9.a)$$

$$\phi_{Q1D}(\omega)\approx\frac{1}{\sqrt{2D_{/\!/}D_\perp}}=\text{const.}, \quad \text{for} \quad \omega\ll D_\perp. \quad (2.9.b)$$

Equation (2.9.a) demonstrates the typical 1D behavior of $1/\sqrt{\omega}$ and eq. (2.9.b) that of 3D behavior, as commonly found in the conducting polymers. Since the actual systems are three-dimensionally anisotropic, 2D behavior described by log ω can appear between 1D and 3D regimes.[29-31]

2.3.2 *Effect of delocalized wave function*

In the case of the neutral soliton in pristine *trans*-polyacetylene, eq. (2.7) should be used instead of the abbreviated eq. (2.8), since its wave function is delocalized by the half-width $L\sim 7$ ($c_{/\!/}$) that is large enough to violate the criterion $\omega\ll D_{/\!/}c_{/\!/}^2/\Delta r_{eff}^2$ (§2.3.1) at high frequencies due to an increase of Δr_{eff} caused by the delocalization. In such a case, the correction factor $\exp\{-2L_{eff}\sqrt{\omega/2D_{/\!/}}\}$ should be multiplied to eq. (2.8), where L_{eff} is the effective delocalization length equal to γL in ref. 32. This expression overestimates the correction at higher frequencies because of insufficient approximation. Figure 2 shows the corrected behavior of $2D_{/\!/}\phi_{Q1D}(\omega)$ as a function of $\sqrt{2D_{/\!/}/\omega}$. Such a correction produces a downward shift of $\phi_{Q1D}(\omega)$ by $2L_{eff}\sqrt{\omega/2D_{/\!/}}$ at low-frequencies, resulting in a finite intercept of the abscissa when extrapolating the slope in the low frequency range. Since this intercept is proportional to L_{eff}, it has been proposed to estimate the neutral soliton width in *t*-(CH)$_x$ by ^{1}H NMR.[25,32] In the case of the Su-Schrieffer-Heeger (SSH) soliton[33] with the full width of L_{SSH} at half-maximum, we estimated the effective length to be $L_{eff}/L_{SSH}\sim 0.4$ for the electron-electron dipolar and ~ 0.5 for the contact hyperfine interac-

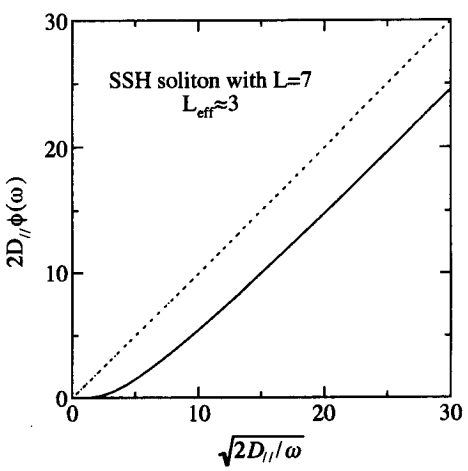

Fig. 2. The spectral density $J(\omega)$ with delocalized wave function as a function of $\sqrt{2D_{/\!/}/\omega}$ at higher frequency than $D_\perp$, where $L_{eff}=3$ estimated for the SSH soliton with $L=7$ is used.

tions, which is larger than $L_{\mathrm{eff}}/L_{\mathrm{Box}}\sim 0.33$ for the box-shaped soliton.[32] Equation (2.7) is also useful for discussing the effect of finite chain length, as will be described in §2.5.

2.4 *Spin-lattice (T_1^{-1}) and spin-spin (T_2^{-1}) relaxation rates*

Expressions for T_1^{-1} and T_2^{-1} are given by

$$\begin{aligned} T_1^{-1}&=\frac{3}{2}\gamma_S^4\hbar^2S(S+1)[J^{(1)}(\omega_0)+J^{(2)}(2\omega_0)]\\ &=\gamma_S^4\hbar^2S(S+1)c\Sigma_l[0.2\phi(\omega_0)+0.8\phi(2\omega_0)]\\ &=3\gamma_S^2k_BT\chi\Sigma_l[0.2\phi(\omega_0)+0.8\phi(2\omega_0)] \end{aligned} \tag{2.10}$$

and

$$\begin{aligned} T_2^{-1}&=\frac{3}{8}\gamma_S^4\hbar^2S(S+1)[J^{(0)}(0)+10J^{(1)}(\omega_0)+J^{(2)}(2\omega_0)]\\ &=\gamma_S^4\hbar^2S(S+1)c\Sigma_l[0.3\phi(0)+0.5\phi(\omega_0)+0.2\phi(2\omega_0)]\\ &=3\gamma_S^2k_BT\chi\Sigma_l[0.3\phi(0)+0.5\phi(\omega_0)+0.2\phi(2\omega_0)] \end{aligned} \tag{2.11}$$

in the case of the electron-electron dipolar interaction.[28] The susceptibility χ is in units of emu per unit molecule. At the second equality of eqs. (2.10) and (2.11), the powder average of $J^{(j)}$'s was taken, resulting in the lattice sum over r_1 and r_2 described by $\Sigma_l=\Sigma P_2(\cos\theta_{12})/(r_1^3r_2^3)$.[29] Determination of $D_{/\!/}$ requires precise information on the lattice constants to avoid ambiguity caused by Σ_l. This point is in contrast to the case of $D_\perp$ which could be obtained graphically and thus more definitely. The spin-spin relaxation rate T_2^{-1} can be observed as a broadening of the ESR peak-to-peak linewidth $\Delta H_{\mathrm{pp}}=2T_2^{-1}/(\sqrt{3}\gamma_S)$, and can be written as the sum of the two terms $T_2'^{-1}\propto 0.3\phi(0)$ and $T_1'^{-1}\propto 0.5\phi(\omega_0)+0.2\phi(2\omega_0)$. The first one, three-tenths of T_2^{-1} at $\omega=0$, is the electron-electron dipolar broadening narrowed by the rapid diffusive motion and is independent of frequency. The second one, seven-tenths of T_2^{-1} at $\omega=0$, is produced by the rapid spin-lattice relaxation mechanism, called lifetime broadening, and depends on the frequency in a somewhat different manner from T_1^{-1}. In the 3D regime at $\omega\ll D_\perp$, T_2^{-1} is expected to become equal to T_1^{-1}, as was found experimentally in pristine *trans*-polyacetylene.[34] The ESR linewidth measurement is suitable for studying the spin dynamics, because it is easier to measure with high accuracy than T_1^{-1}.

When we analyze the ESR linewidth, there is one important point to be aware of; additivity of the ESR linewidths. If all the sources for the linewidth have Lorentzian line shape, one can apply the simple algebraic addition rule. In the case of the sum of Lorentzian and Gaussian line shapes, it is required to deconvolute the observed shape to obtain each linewidth. In many of the actual systems, the motion of the spins is rapid enough to satisfy the extreme narrowing condition where Lorentzian shape is expected for the line shape. In the case of the width due to trapping, as discussed in §4.2, however, the line shape has been found to deviate from Lorentzian. Then, in quantitative analysis one should take account of the additivity of the two contributions. Such a deviation was found in pristine t-$(CH)_x$ well below 100 K. As an actual problem, however, the deviation from Lorentzian is not so serious as to cause deviation of the raw data out of the experimental error range.

2.5 *Effect of finite chain length*

In this section we will discuss the effect of finite conjugation length l. Spin is expected to diffuse by an average distance of $x(t)=c_{/\!/}\sqrt{D_{/\!/}t}$ for time t. Then, if the frequency is sufficiently higher than the characteristic frequency $\omega_c=D_{/\!/}c_{/\!/}^2/l^2$, the finite conjugation length l would have no effect on our earlier discussion since the spins cannot know the presence of chain ends. If the frequency, however, is lower than ω_c, providing that $D_\perp\ll\omega_c$, the earlier discussion that $1/\tau_c=D_\perp$ should be modified; $\omega_c=D_{/\!/}c_{/\!/}^2/l^2$ instead of $D_\perp$ determines $1/\tau_c$. To proceed further in the discussion of the effect of the finite chain length, we start with

$$\Phi_{\mathrm{Q1D}}(r_1,r_2,t)\approx\frac{\exp(-2D_\perp t)}{\sqrt{4\pi D_{/\!/}\omega}} \tag{2.12}$$

for the probability density $\phi_{\mathrm{Q1D}}(\omega)$. We can take into account the effect of l by multiple reflections at the chain ends as

$$\begin{aligned} \Phi_{\mathrm{Q1D}}(r_1,r_2,t)=\frac{\exp(-2D_\perp t)}{\sqrt{4\pi D_{/\!/}\omega}}\Bigg\{1+2\sum_{n=1}^{\infty}\exp\left(-\frac{n^2N^2}{D_{/\!/}t}\right)\\ +\frac{2}{N}\sum_{m=0}^{N-1}\sum_{n=0}^{\infty}\exp\left(-\frac{\left(n+\frac{m}{N}\right)^2N^2}{D_{/\!/}t}\right)\Bigg\}, \end{aligned} \tag{2.13}$$

where $N=l/c_{/\!/}$ is the number of conjugated monomer units and m is the site number of interest, which is numbered from the chain end. The second term is a sum for the even-number reflections at the chain ends and the third term is that for the odd-number reflections. Since each m site is not equivalent in the case of odd-number reflections, they should be averaged out. Figure 3 shows the calculated autocorrelation function $G(t)$ multiplied by $\sqrt{4\pi D_{/\!/}\tau_\perp}$ with the parameter $K=N/\sqrt{D_{/\!/}\tau_\perp}$ as a function of the time normalized by $\tau_\perp$. When $K\gg 1$, a

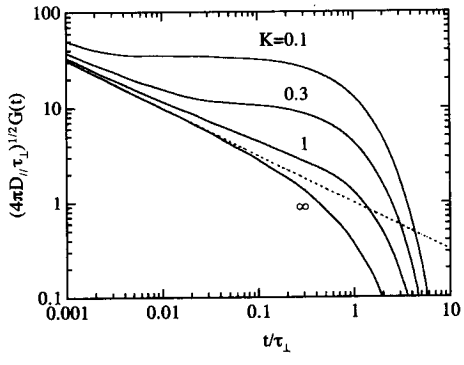

Fig. 3. The autocorrelation functions $\sqrt{4\pi D_{/\!/}\tau_\perp}G(t)$ for the finite chain length. $K=N/\sqrt{D_{/\!/}\tau_\perp}$ is the chain length normalized by the mean distance of diffusion for the interchain escape time $\tau_\perp$.

cutoff of $G(t)$ at $t \approx \tau_\perp$ is caused by $D_\perp = 1/\tau_\perp$, but when $K \ll 1$, $G(t)$ levels off at $t = K^2\tau_\perp = N^2/D_{/\!/}$, i.e., a saturation of the correlation of motion occurs as an effect of the finite chain length l. In Fig. 4 the corresponding normalized Fourier spectrum $\phi(\omega)/(\omega_c N)$, which levels off below $\omega \sim 5\omega_c$, is shown for the pure 1D case of $\tau_\perp = \infty$ where $\omega_c = D_{/\!/}/N^2$ acts as a new cutoff frequency instead of $D_\perp$.[35]

This effect of the finite chain length gives a lower bound of the chain length $l_{\min} = \sqrt{D_{/\!/}\tau_\perp c_{/\!/}} \leq \sqrt{D_{/\!/}/\omega_c c_{/\!/}} = l$ under the condition that the observed $\tau_\perp^{-1}$ is always equal to or larger than ω_c and $D_\perp$. The estimated $l_{\min}$ is summarized in Table I.

Some calculations have been reported using anisotropic random walk on the cases of finite chain length and/or a delocalized wave function.[35,36]

3. Experimental

The most characteristic feature of this experiment is the wide frequency range from several MHz to 24 GHz. To avoid systematic error the same sample should be used throughout the whole frequency range, because the relaxation rate of electron spin in the conducting polymers is usually sensitive to sample handling, especially residual oxygen contamination.

As shown in eqs. (2.10) and (2.11), both T_1^{-1} and T_2^{-1} are useful in studying the spin dynamics. T_1^{-1} is a basic parameter, but is not easy to study in the wide frequency range, mainly because of shorter relaxation time than dead times of the spectrometers particularly at lower frequency. Thus, we must use a saturation technique at less than 500 MHz at room temperature. On the other hand, T_2^{-1} or the linewidth is easy to study and to determine precisely. Therefore, T_2^{-1} is usually used for spin dynamics study. A least squares fit of the Lorentzian line shape is applied to attain a high relative resolution of milligauss order. Determination of the relative magnetic field is done by monitoring the sweep rate of the magnetic field which is detected by a large coil wound around pole pieces of an electromagnet. In actual measurement, sufficient attention has been paid to the saturation effect of a strong radio-frequency field and excess broadening by magnetic field modulation.

A block diagram of the home-built spectrometer is shown in Fig. 5. This configuration is common to all the frequencies, except for the loop-gap resonators in the GHz range[37] and the usual cylindrical cavity at 24 GHz.

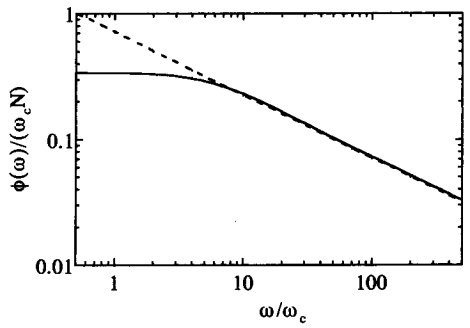

Fig. 4. The Fourier spectrum $\phi(\omega)/(\omega_c N)$ of the autocorrelation function $G(t)$ in the case of a 1D system, that is, $\tau_\perp = \infty$ or $D_\perp = 0$. Note that $\phi(\omega)$ levels off below $\omega \sim \omega_c$.

Table I. The estimated minimum conjugation length $l_{\min}$ in several conducting polymers.

	Polyacetylene	Polyaniline	Polythiophene
$l_{\min}$ $(c_{/\!/})$	1.0×10^3	180	580

4. Neutral Soliton Dynamics in Pristine Trans-Polyacetylene

4.1 *ESR T_1^{-1} and T_2^{-1} (linewidth)*

As the first example of spin dynamics study by ESR, neutral soliton dynamics in pristine *trans*-polyacetylene should be discussed because the relaxation mechanism has been identified, for the first time in this system, to be the dipolar interaction between the electron spins and the hyperfine interaction.[8]

Figure 6 shows the spin-lattice relaxation rate T_1^{-1} versus frequency for both *t*-$(CH)_x$ and *t*-$(CD)_x$ measured by the saturation technique. The solid curves are predictions of eq. (2.10), fitted by a least squares method to the experimental data. Although *t*-$(CH)_x$ and

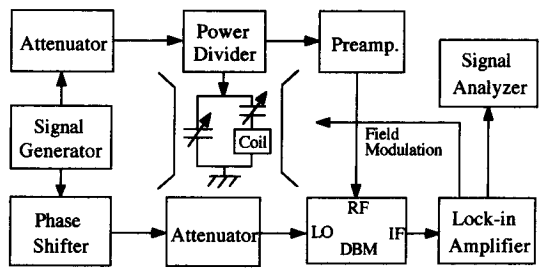

Fig. 5. The block diagram of the home-built ESR spectrometer for various frequencies. The loop-gap resonator in the GHz range and the cylindrical cavity at 24 GHz was used instead of the coil at lower frequencies.

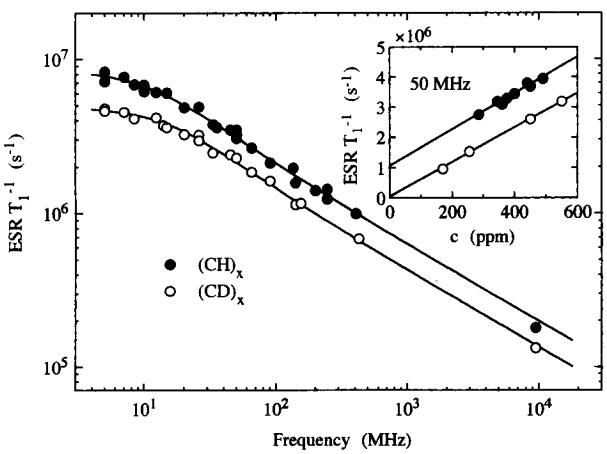

Fig. 6. The frequency dependence of the spin-lattice relaxation rates at room temperature in *t*-$(CH)_x$ and *t*-$(CD)_x$ measured by the saturation technique. Inset: T_1^{-1} as a function of spin concentration c (ppm) for both *t*-$(CH)_x$ and *t*-$(CD)_x$. Note the well-defined difference at $c = 0$ between *t*-$(CH)_x$ and *t*-$(CD)_x$, which comes from the hyperfine interaction with the proton or deuteron.

t-$(CD)_x$ show similar frequency dependence, there is a considerable difference in their magnitude. The inset of Fig. 6, showing the spin concentration dependence of the relaxation rate for both t-$(CH)_x$ and t-$(CD)_x$, clearly elucidates that this difference is caused by two different contributions: the electron-electron dipolar interaction and the hyperfine interaction. Firstly, T_1^{-1} proportional to the spin concentration c should be the dipolar interaction between the spins, as predicted by eq. (2.10), and secondly, T_1^{-1} independent of c should be the hyperfine interaction with protons or deuterons. Since these two isotopes contribute to T_1^{-1} with different weights according to $\gamma_n^2 I_n(I_n+1)$,[9] the ratio of T_1^{-1} for t-$(CH)_x$ to that for t-$(CD)_x$ would be proportional to the ratio of $\gamma_H^2 I_H(I_H+1)$ to $\gamma_D^2 I_D(I_D+1)$ which is as large as 16. This ratio is consistent with the experimental ratio of T_1^{-1} at the concentration extrapolated to zero. Therefore, one can conclude that the relaxation mechanism of ESR T_1^{-1} is dominated by the electron-electron dipolar interaction in t-$(CD)_x$, but by both the dipolar and the hyperfine interactions in t-$(CH)_x$.

It is apparently possible to interpret the $1/\sqrt{\omega}$ dependence of T_1^{-1} in Fig. 6 as a spin diffusion due to exchange coupling in a one-dimensional fixed spin chain model. However, the spin concentration of less than 1 spin per 2000 carbon atoms in *trans*-polyacetylene is too low to explain ESR T_1^{-1} by such a model.[38] When one assumes unrealistically that the spins form clusters to increase the effective spin concentration, the concentration dependence shown in the inset of Fig. 6 cannot be accounted for because with increasing spin concentration, the exchange and dipolar interactions rather increase, which results in an increase of the diffusion rate along the chain, and equivalently, a decrease of T_1^{-1} as expected from eqs. (2.8) and (2.10), which is contradictory to the observed dependence in Fig. 6.

The overall feature of the spectral density described by eq. (2.8) could not be obtained experimentally only by T_1^{-1} because of two experimental limitations. The first is inapplicability of the saturation technique below 100 K, where the line shape of ESR in the pristine polyacetylene becomes slightly inhomogeneous, preventing reliable analysis of the data. The second is the presence of intrinsic finite dead time in the pulse technique, which limits measurements to T_1^{-1} longer than $1/\omega$. Therefore, we developed the ESR linewidth analysis as a new method of spin dynamics study.[12] Figures 7(a) and 7(b) show the temperature dependence of the ESR linewidth in t-$(CH)_x$ and t-$(CD)_x$ versus $1/\sqrt{f}$. The solid curves show the sum of eq. (2.11) and the constant term ΔH_{trap}, fitted to the experimental data less than $1/\sqrt{f} \approx 0.4\ MHz^{-1/2}$ or higher than $f \approx 6$ MHz by the least squares method. Both the constant term ΔH_{trap} and the steep increase below 6 MHz that are not predicted by eq. (2.11) are related to trapping of the neutral soliton.

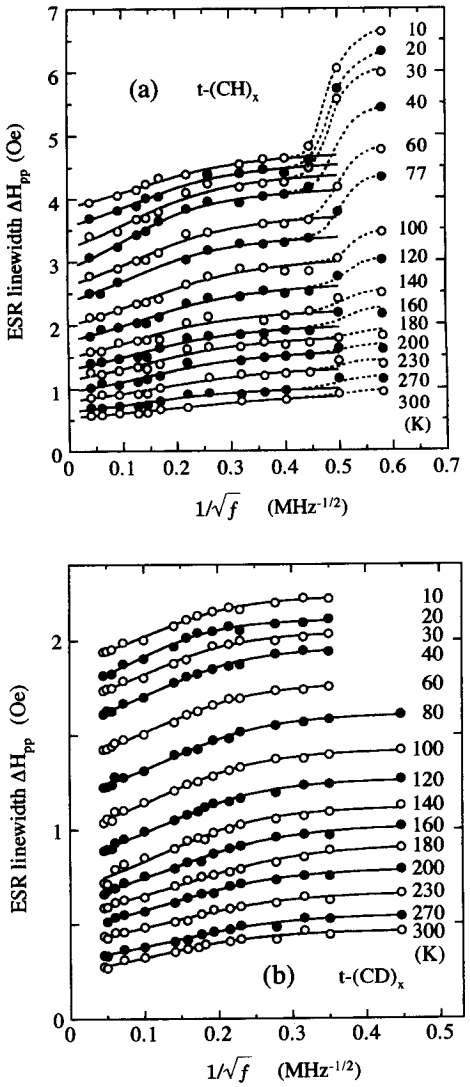

Fig. 7. The frequency dependence of ESR linewidth for (a) t-$(CH)_x$ and (b) t-$(CD)_x$ with the implicit parameter of temperature. Note that anomalous line broadening is found at frequencies lower than 6 MHz ($1/\sqrt{f} \approx 0.4$) only in t-$(CH)_x$, as confirmed in Fig. 10.

4.2 *Effect of trapping*

4.2.1 *Diffuse/trap model*

It is well known that *cis*-$(CH)_x$ has a small number of neutral solitons that are localized (trapped) within a short *trans* segment. The ESR spectrum of such a soliton is intrinsically inhomogeneous (static).[39] This finding suggests a new idea[25] in interpreting the ESR linewidth in t-$(CH)_x$: the neutral soliton diffuses rapidly most of the time (diffusing state), but it is sometimes trapped for a period longer than $1/D_{//}$ at special trapping sites (trapped state), for example, the sites affected by the potential of oxygen adsorbed on sample surfaces[25] and of the residual catalyst.[16,20] For such a period in the trapped state, the same broadening mechanism as in the *cis*-$(CH)_x$ becomes effective. This is called the diffuse/trap model[2] in this review.

According to this model, the width due to trapping ΔH_{trap} is given by $c_{tr}\Delta H_h + c_{tr}^2 \Delta H_d$. Here, c_{tr} is the probability of the soliton being in the trapped state, which is temperature dependent through the trapping potential energy E_{trap}, and ΔH_h and ΔH_d are the *static* hyperfine and dipolar widths, respectively, at absolute zero. Using $\Delta H_{trap} = 1.41$ Oe[11] and 3.7 Oe[12] for t-$(CD)_x$ and t-$(CH)_x$, respectively, as shown in Fig. 8, ΔH_h was

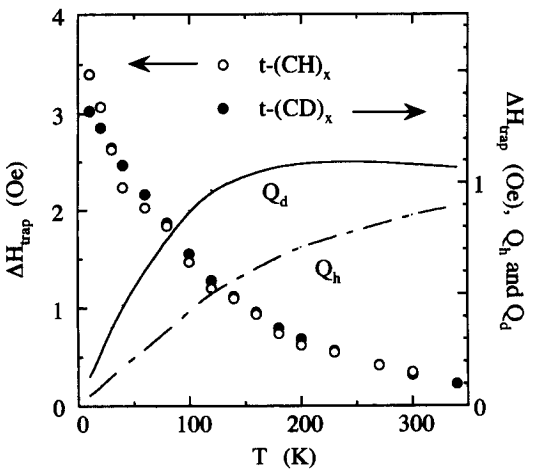

Fig. 8. The temperature dependence of the width due to trapping (the constant contribution in Fig. 7) in t-$(CH)_x$ and t-$(CD)_x$ and the correction factor for trapping; the broken curve, $Q_h=c_{diff}=1-c_{tr}$, and the solid curve, $Q_d=1+0.83c_{tr}-1.83c_{tr}^2$.

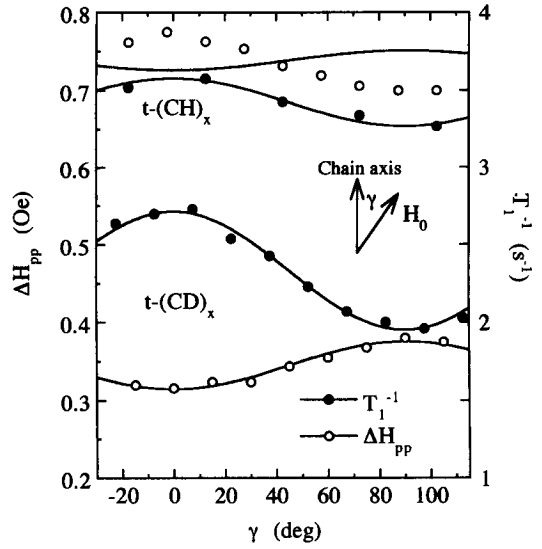

Fig. 9. ESR T_1^{-1} and linewidth versus the angle of magnetic field to the chain direction in the partially stretch-aligned t-$(CH)_x$ and t-$(CD)_x$ samples. A reversed pattern phase of linewidth $\Delta H_{pp} \propto (1+3\cos^2\gamma)$ against $T_1^{-1} \propto (5-3\cos^2\gamma)$ is expected from eqs. (2.10) and (2.11) as shown by the solid curves.[10] In the case of t-$(CH)_x$, however, the pattern phase of the linewidth is dominated by the width due to trapping, similarly to that for *cis*-$(CH)_x$ given in ref. 39.

estimated as 0.87 Oe and 3.16 Oe for t-$(CD)_x$ and t-$(CH)_x$, respectively, and $\Delta H_d=0.54$ Oe.[17] Using these values, we can estimate the number of solitons diffusing as $c_{diff}=1-c_{tr}$ at each temperature and the intrinsic T_2^{-1} using the correction factors Q_h and Q_d for the hyperfine and dipolar interactions, respectively. Here, $Q_h=c_{diff}$ and $Q_d=[c_{diff}+\sqrt{2}\,c_{tr}]c_{diff}+\sqrt{2}\,c_{tr}c_{diff}\approx 1+0.83c_{tr}-1.83c_{tr}^2$.[11,17,23-25] The parameters Q_h and Q_d obtained experimentally are shown as a function of temperature for t-$(CD)_x$ in Fig. 8.

This model make it possible to interpret all the available data consistently.

4.2.2 *Anisotropy of ESR T_1^{-1} and linewidth*

ESR T_1^{-1} and linewidth in stretch-aligned polyacetylene show anisotropic sinusoidal behavior.[10] The solid curves in Fig. 9 show the predictions of eqs. (2.10) and (2.11) (the first line in each equation) for diffusing spins. As for T_1^{-1}, the phases of patterns both in t-$(CH)_x$ and t-$(CD)_x$ are the same and consistent with eq. (2.10). For the linewidth, the phase of anisotropy pattern for diffusing spins is the reverse of that for the localized spin, similarly to that in *cis*-$(CH)_x$.[10] Figure 9 shows that the pattern for the linewidth in t-$(CD)_x$ is that of diffusing spins, but that in t-$(CH)_x$ is of the localized spins, similarly to in *cis*-$(CH)_x$. This difference can be interpreted as the difference of γ_n in magnitude for the proton and the deuteron. In t-$(CH)_x$, the anisotropy pattern was dominated by the width ΔH_{trap} due to trapping, instead of T_2^{-1} described by eq. (2.11), through the large hyperfine coupling with the proton nuclei, but eq. (2.11) governs the linewidth in t-$(CD)_x$ by virtue of the small hyperfine coupling with the deuteron.

4.2.3 *Anomalous broadening below 6 MHz in t-(CH)$_x$*

Anomalous broadening of the linewidth below 6 MHz was observed only in t-$(CH)_x$ (Fig. 7(a)), not in t-$(CD)_x$ (Figs. 7(b) and 10(b)). This can be understood as an increase of the trapping width ΔH_{trap} due to a crossover from unlike spins to like spins with the frequency passing through the effective hyperfine coupling constant a_{eff} in units of frequency.

Effective hyperfine coupling constant a_{eff} is a product of the spin density and the coupling constant per electron spin. When the resonance angular frequency ω in ESR is larger than a_{eff}, the secular term AS_zI_z is effective for broadening, but the spin flip-flop term $BS_\pm I_\mp$ is ineffective because of decoupling by the strong external magnetic field H_0 (refer to eq. (2.2) and ref. 28). This situation is called "unlike spins" that have distinctly different resonance frequencies. When ω, however, becomes smaller than a_{eff}, such a decoupling becomes ineffective, since each Larmor frequency is governed not by the external field, but by the effective hyperfine coupling frequency. The electron and the proton spins in such a state are called "like spins". Therefore, the linewidth is broadened additionally by the spin-flip term $BS_\pm I_\mp$ at frequency lower than a_{eff}.

Since the $BS_\pm I_\mp$ term has a similar coefficient to the AS_zI_z term,[28] the phase of anisotropy patterns with and without the $BS_\pm I_\mp$ term should be the same. Actually, the anisotropy pattern observed below 6 MHz has the same phase as that above 6 MHz, as shown in Fig. 10. In addition, the ratio of additional broadening due to the $BS_\pm I_\mp$ term to that due to the AS_zI_z term is expected to be 0.5.[28] This value is also consistent with the observed ratio $\Delta H_{exc}/\Delta H_{trap}=1.9/3.4\approx 0.56$ at 10 K. Therefore, we concluded that this mechanism is the origin of the observed anomalous broadening below 6 MHz in t-$(CH)_x$. To render this mechanism effective, the condition $t_{trap}\geq 1/a_{eff}$ ($\sim 10^{-7}$ s) should be satisfied, where t_{trap} is the time during which the neutral soliton stays at the trapping site.

Since about 90% of ΔH_{trap} is due to hyperfine coupling with the proton nuclei at 10 K, this crossover frequency of 6 MHz gives an estimate of $\rho_s \geq 0.1$ spins/

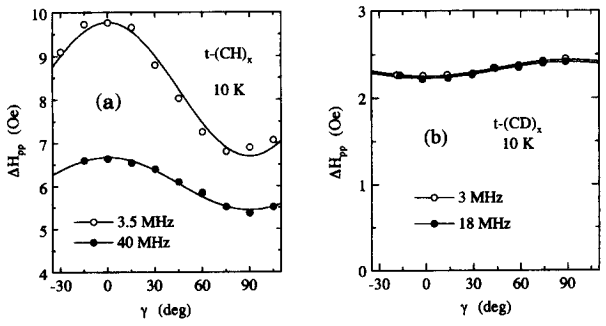

Fig. 10. The angular dependence of ESR linewidth at 10 K (a) with frequencies 40 MHz (without the excess width) and 3.5 MHz (with the excess width) in t-$(CH)_x$ and (b) 18 MHz and 3 MHz in t-$(CD)_x$. Note that the excess linewidth shows the same phase of pattern as that for cis-$(CH)_x$, similarly to the width due to trapping.

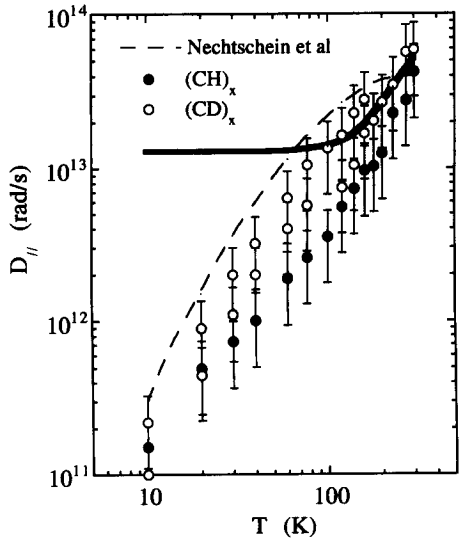

Fig. 11. The temperature dependence of the diffusion rate along the chain, $D_{/\!/}$, for t-$(CH)_x$ and t-$(CD)_x$ together with that determined by ^{1}H NMR.[25] The solid curve indicating $D_{/\!/}$ for t-$(CD)_x$ before the trapping correction shows a negligibly small contribution due to trapping above 100 K.

carbon for the maximum spin density of the neutral soliton in *trans*-$(CH)_x$,[12] providing that the hyperfine coupling constant is -23 Oe/spin with the proton nuclei. This figure is consistent with the estimate by the ENDOR technique that $\rho_s=0.1$–0.19 spins/carbon for *cis*-$(CH)_x$,[40] but is inconsistent with the uniformly delocalized wave function from 40 to 60 carbon sites.[41] Then, the present analysis for the maximum spin density and the ENDOR data are consistent with the SSH-type wave function for the neutral soliton in both *cis*- and *trans*-$(CH)_x$, except for the negative spin polarization in odd carbon sites due to the Coulomb correlation.[40,42]

Finally we would like to stress that the linewidth, being the true basic parameter in ESR, is clearly analyzed on the basis of the interesting idea of trapping, including the frequency dependence of the linewidth. This experimental finding suggests that in the interpretation of neutral soliton dynamics in *trans*-polyacetylene, the trapping effect plays a very important role, and that conclusions not taking into account the trapping effect should be viewed with care.

4.3 *Temperature dependence of diffusion rates*

The experimental data shown in Figs. 6 and 7 yielded the diffusion rates along ($D_{/\!/}$) and across ($D_\perp$) polymer chains by a least squares fit to eqs. (2.10) and (2.11), as shown by the solid curves. $D_{/\!/}$ is inversely proportional to the initial slope and $D_\perp$ is the transition frequency from the 1D (linear increase) to the 3D (leveling off) regimes in Fig. 7. The temperature dependences of $D_{/\!/}$ in t-$(CH)_x$ and t-$(CD)_x$ are shown in Fig. 11 together with the data analyzed by ^{1}H NMR.[23–25] Here, the solid curve shows $D_{/\!/}$ without correction of the trapping effect, whereas the other symbols include it. Note that $D_{/\!/}$ above 100 K is almost free of the trapping effect, as shown by the solid curve.

Figure 11 suggests that the dynamics of the neutral soliton is not a free ballistic motion at low temperature, but a hopping driven by phonons to overcome some attractive potentials, which follows T^2 dependence.[10,12] It is interesting to know that the result by proton NMR[23–25] is consistent with that by ESR. If we take into account quantitative large ambiguity induced from the diffuse/trap model (especially in proton NMR, almost the entire temperature dependence is governed by the trapping effect), this agreement is satisfactory and suggests that both of the methods detected the same phenomenon, in spite of the criticism that $1/\sqrt{f}$ dependence observed by proton NMR could come from a relaxation mechanism other than the neutral soliton diffusion.[43] As for the temperature dependence of $D_{/\!/}$, many theoretical approaches have been made.[44,45]

Figure 12 shows the temperature dependence of the cutoff frequency $1/\tau_\perp$ in t-$(CD)_x$. It is interesting to consider the origins of the cutoff frequency, because a topological kink of the neutral soliton is essentially localized on the chain. Possible origins are due to (1) an exchange interaction between the electron spins[46] and (2) soliton hopping from the neutral soliton to the charged soliton proposed by Kivelson.[47] Then, a possible explanation of Fig. 12 is as follows. In the temperature range below 100 K, mechanism (1) of the exchange interaction governs $1/\tau_\perp$. At the lowest temperature most of the neutral solitons are trapped and several solitons accumulate around residual catalysts and adsorbed oxygens, which enhances the exchange interaction among them. With increasing temperature, the neutral solitons start to diffuse rapidly, which decreases the efficiency of the exchange interaction among the neutral solitons. In a higher temperature range, neutral soliton hopping via the charged solitons assisted by the phonon becomes dominant. Kivelson suggested a strong temperature dependence for the conductivity $\sigma \propto T^{13}$ in this mechanism, which is similar to the rapid increase of $1/\tau_\perp$ around room temperature.

It is well known that Naarmann-type polyacetylene (NT-PA) shows higher electrical conductivity than the Shirakawa-type one (S-PA). The origins of this difference are still under study.[48–50] Recently, Wang *et al.* reported that the interchain cutoff frequency $1/\tau_\perp$ in

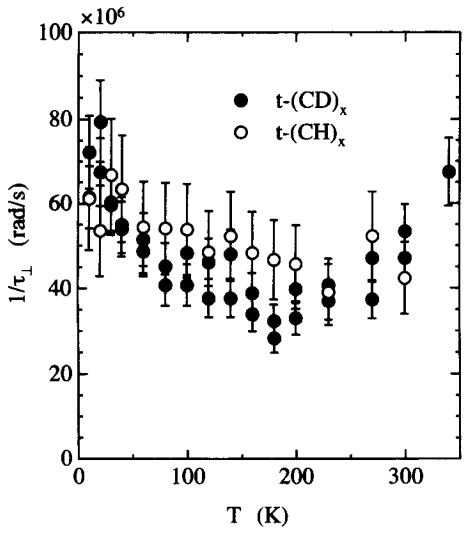

Fig. 12. The temperature dependence of the cutoff frequency $\tau_\perp$ for t-$(CH)_x$ and t-$(CD)_x$.

pristine polymer is related to this difference.[51] To confirm this interpretation, $1/\tau_\perp$ was studied in both types of the polyacetylene and no meaningful difference between them was found in $1/\tau_\perp$, but a correlation between $D_{/\!/}$ and $\Delta H_{\rm trap}$ was found, suggesting a higher number of trapping centers in NT-PA than in S-PA, as shown in Table II.[16] This shows that the origin of the difference between the two in conductivity is not related to $1/\tau_\perp$ in *trans*-polyacetylene, but rather to the degree of chain orientation in these polymers.[16,20,49,50]

We can try to estimate the lower bound $l_{\rm min}$ for the average conjugation length in t-polyacetylene; $l_{\rm min}=\sqrt{D_{/\!/}\tau_\perp}c_{/\!/}=\sqrt{5\times10^{13}\cdot2\times10^{-8}}c_{/\!/}=10^3c_{/\!/}$. Here, we used the parameters at 300 K. The estimated conjugation number is the minimum value, at least for chains carrying a neutral soliton.

4.4 *Relation to pulse ESR experiments*[17]

In the studies of spin dynamics, some pulsed ESR experiments have been reported: the electron spin echo (ESE) phase memory time $T_{\rm M}$ which is a parameter similar to T_2^{-1},[52] the free induction decay (FID) studies,[53] the spin-lattice relaxation rate T_1^{-1},[54] and the ESE-detected multiple-quantum NMR (ESE-MQNMR).[55] All the experiments were done mainly at the X-band (~9 GHz). The authors of those papers reported conclusions incompatible with each other. It seems probable that the trapping effect was not taken into account in their analyses with independent models. Relaxation data T_1^{-1} and $T_{\rm M}^{-1}$ measured only at a few frequencies are not enough to reveal the neutral soliton dynamics in t-polyacetylene. The observed relaxation phenomena can not be attributable only to a unique mechanism; there are other contributions such as the width due to trapping and the effect of the delocalized wave function. FID is the same as the line shape in nature. Both the FID and the line shape analysis should be considered with great care, because very small amplitude of the signal tails includes important information which is sensitive to many other perturbing factors, for example, trapping.

4.4.1 *Spin-echo decay time T_M*

Figure 13 shows the temperature dependence of the motionally narrowed ESR linewidth $(\gamma T_2')^{-1}\propto0.3\phi(0)$ and the phase memory width $(\gamma T_{\rm M})^{-1}$ in t-$(CD)_x$.[52,56] Here, $(\gamma T_2)^{-1}$ can be written as a sum of the two parts, $(\gamma T_1'(\omega))^{-1}$ and $(\gamma T_2')^{-1}$, the nonsecular (lifetime) width and the secular width, respectively. Here, note that $(\gamma T_2')^{-1}$ does not decrease monotonically with T as is usually found in motional narrowing of 3D materials, but is proportional to $1/\sqrt{2D_{/\!/}D_\perp}$, as seen in eq. (2.9.b). Figure 13 will be interpreted as further evidence for neutral soliton trapping.

The authors of ref. 52 analyzed the phase memory time with the stationary Gaussian spectral diffusion formalism and concluded that the diffusion rate is smaller by several orders of magnitude than that estimated from the frequency dependence of ^{1}H NMR T_1^{-1}. This conclusion is refuted by the present spin dynamics study using frequency dependence. Our conclusion is that the spin-echo decay rate undergoes a crossover from $\Delta H_{\rm trap}+(\gamma T_2')^{-1}$(=ESR linewidth at X-band) above 200 K to $(\gamma T_2')^{-1}$ below 100 K, as can be seen from Fig. 13. The reason is as follows.

$T_{\rm M}$ due to trapping is roughly defined as the time for the accumulated dephasing angle of spin packets in x^*-y^* rotating coordinates to reach one radian, $\gamma(H_{\rm loc}c_{\rm tr})T_{\rm M}\approx1$ due to the effective local field $H_{\rm loc}c_{\rm tr}$[28] which can be observed as the width due to trapping, $\Delta H_{\rm trap}\approx H_{\rm loc}c_{\rm tr}$. Here, $H_{\rm loc}$ is the local magnetic field at the neutral soliton and $c_{\rm tr}$ is the probability for the neutral soliton to be in the trapped state, as defined in §4.2.1. $c_{\rm tr}$ changes with temperature, as shown in Fig. 8. Although the width due to trapping $\gamma H_{\rm trap}=\gamma H_{\rm loc}c_{\rm tr}$ is always much greater than $T_2'^{-1}$ in polyacetylene, $H_{\rm loc}$ may not necessarily contribute to $T_{\rm M}^{-1}$ because a static local field exerts no effect on $T_{\rm M}^{-1}$. Therefore, $t_{\rm trap}\ll T_2'$ is another criterion for $\Delta H_{\rm trap}$ not to be canceled by the spin-echo focusing pulse, but to contribute to $T_{\rm M}^{-1}$.[28] Here, $t_{\rm trap}$ is the average duration of stay at a trapping

Table II. The diffusion rate along the chain (on-chain), $D_{/\!/}$, and across the chain (off-chain), $D_\perp$, the residual linewidth $\Delta H_{\rm trap}$ caused by the trapping of the neutral soliton and the number of spins (neutral soliton) for each sample for different synthesis and isomerization conditions.

Type of PA and isomerization	On-chain diffusion rate $D_{/\!/}$ (10^{13} Hz)	Off-chain diffusion rate $D_\perp$ (10^7 Hz)	Residual linewidth $\Delta H_{\rm trap}$ (Oe)	Number of spins c (10^2 ppm)
NT-PA (180°C 55 min)	5.8(1.5)	1.5(0.4)	0.99(0.02)	5.4(0.3)
S-PA-1 (145°C 2.5 h)	9.0(2.5)	1.3(0.4)	0.69(0.02)	4.4(0.2)
S-PA-2 (165°C 2 h)	12.7(5)	1.4(0.5)	0.66(0.03)	4.4(0.2)
S-PA-3 (180°C 2 min)	12.6(4)	1.7(0.5)	0.22(0.02)	4.3(0.2)

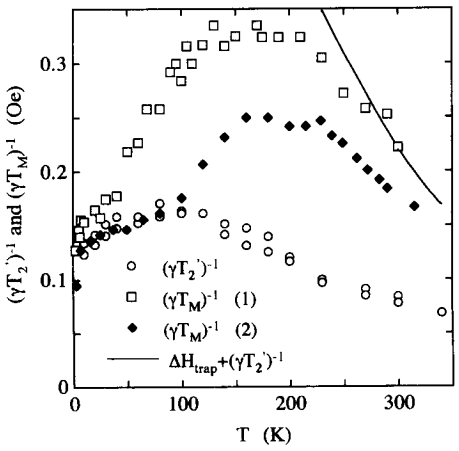

Fig. 13. The temperature dependence of the motional narrowed secular width $(\gamma T_2')^{-1}$ which is approximately equal to $(\gamma T_2)^{-1}$ at the X-band (eq. (2.11)) and the phase memory time T_M obtained by (1) Shiren *et al.*[52] and (2) Isoya.[56] The solid curve shows a typical behavior for $(\gamma T_2')^{-1}+\Delta H_{trap}$. At temperatures lower than 100 K, $(\gamma T_M)^{-1}$ coincides with the secular width $(\gamma T_2')^{-1}\sim(\gamma T_2)^{-1}$ at X-band. At temperatures higher than 200 K, however, $(\gamma T_M)^{-1}$ is governed not only by the secular width $(\gamma T_2')^{-1}$, but also by ΔH_{trap}.

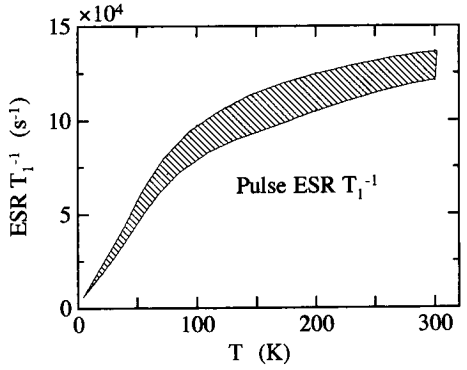

Fig. 14. The schematic temperature dependence of the spin-lattice relaxation rate T_1^{-1} measured at 9.5 GHz by the pulse technique.[43,54]

site for the neutral soliton. Then, if t_{trap} is nearly equal to $T_2'\approx 10^{-6}$ s around 100 K, one can naturally expect that $(\gamma T_M)^{-1}$ approaches $(\gamma T_2')^{-1}$ well below 100 K where $t_{trap}\gg T_2'$, and $\Delta H_{trap}+(\gamma T_2')^{-1}$ well above 100 K where $t_{trap}\ll T_2'$, as observed in Fig. 13. This trapping time of $\approx 10^{-6}$ s around 100 K is also consistent with the observation of anomalous excess broadening below 6 MHz in *t*-$(CH)_x$, which requires that t_{trap} meets the condition $t_{trap}\geq 1/a_{eff}\sim 10^{-7}$ s (see §4.2). A definite difference between the two $(\gamma T_M)^{-1}$ data sets is found above 100 K in Fig. 13, implying an extrinsic contribution due to the trapping effect which largely depends on the samples.

The above conclusion directs our attention to the fact that the ESR linewidth is strongly affected by trapping, even if the observed line shape is nearly Lorentzian.

4.4.2 *Spin-lattice relaxation time*

Figure 14 shows the temperature dependence of the spin-lattice relaxation rate T_1^{-1} measured by Robinson *et al.* at the X-band.[54] In the case of T_1^{-1}, the trapping exerts no direct effect, but affects T_1^{-1} indirectly through the delocalized wave function of the neutral soliton combined with the slowing of the diffusion rate $D_{/\!/}$. As discussed in §2.5, this effect strongly suppresses T_1^{-1} at higher frequencies, as shown in Fig. 2.

The authors of ref. 54 proposed a model *without trapping* in which the following apply.

(1) The neutral soliton is delocalized dynamically over 50 sites in a rectangular area, and in such a rectangular region,

(2) the neutral soliton takes on ballistic motion interrupted by phonon scattering, i.e., $D=V_F^2\tau$-like metallic electrons, and then the diffusion rate decreases with increasing T.

(3) Furthermore, diffusive motion of such a rectangular region would be activated thermally.

The last term (3) is proposed to explain motional narrowing of ESR linewidth, compatibly with the restriction (2).

Within the present framework of spin dynamics with the two effects, the trapping (§4.2) and the delocalization effects with the SSH soliton (§2.3.2), the behavior of T_1^{-1} in Fig. 14 is almost reproducible, except for the gradual increase above 100 K. In contrast, the above model fails to explain the ESR linewidth as functions of the frequency and the temperature shown in Fig. 7, as follows.

The ballistic motion of the spin in assumption (2) is inconsistent with the presence of the width ΔH_{trap} due to trapping. In particular, the anomalous broadening below 6 MHz in *t*-$(CH)_x$ could not be explained by the ballistic motion of Spin without the trapping effect (§4.2.3), since the duration for which the electron spin stays in a certain site is too short to couple with the proton spin; it needs more than $\sim 10^{-6}$ s.

Although the assumption (3) without trapping would be possible to interpret the ESR linewidth at the X-band, a consistent interpretation for the temperature and frequency dependences of the ESR linewidth requires the diffuse/trap model, as discussed in the preceding sections.

4.4.3 *Multiple-quantum spin coherence*

An interesting but sophisticated discussion has been reported wherein all of the spins are localized in 99% ^{13}C-enriched polyacetylene, studied by multiple quantum NMR detected by the ESE technique.[55] This is, however, further experimental evidence for the validity of the diffuse/trap model.

Three pulses, $\pi/2$-τ-$\pi/2$-τ_1-$\pi/2$-τ_2, were applied to the electron spin, i.e., the neutral soliton, to induce ^{13}C MQNMR transition only in nuclei coupled to the soliton. Thomann *et al.* found qualitatively the same spectra for *trans*-$(CH)_x$ and *cis*-$(CH)_x$ at 4 and 298 K, demonstrating that the observed spins coherently coupled with $\sim$13 carbon nuclei under all the conditions studied, and as a result, the shape of the neutral soliton is concluded to be the same in each isomer.

If the neutral soliton were diffusing faster than the coupling frequency between the electron spin and the nuclear spin, the multiple quantum coherence would be

destroyed by decoupling of the electron-nuclear interaction. This means that the neutral soliton in the diffusion state could not be observed by this technique, but only the soliton in the trapped state could be observed, that is, the qualitative spectra of this experiment cannot give any information on the existence of the soliton in the diffusing state, but absolute intensity does. The reason why they concluded that "all" the spins were trapped instead of the above was that the ESR signal was composed of only a single species, which requires that "the observed" MQNMR signal should include "all" of the existing spins. Following the diffuse/trap model, however, the ESR signal is composed of a single line and "all" of the spins have an equal chance to contribute to the MQNMR signal in terms of a time sharing of the diffusing and the trapped states. Therefore, *the above experimental result does not indicate whether "all" the solitons were trapped or not* as insisted by them, but, on the contrary, *shows the existence of the soliton in the trapped state even at 298 K*, consistent with the diffuse/trap model of the neutral soliton in pristine polyacetylene.[11,17,25] The temperature dependence of the ESR linewidth ΔH_{trap} due to trapping shown in Fig. 8 predicts that around 10% of the neutral solitons are in the trapped state even at 298 K (more strictly, $t_{\text{trap}} \gg 1/a_{\text{eff}}$ should be satisfied).

Therefore, this technique would be useful in determining how many solitons are trapped at each temperature to check the diffuse/trap model quantitatively. Actually, the reported MQNMR in *trans* isomer has a higher signal-to-noise ratio than in *cis* isomer at 4 K, which is consistent with more than tenfold higher spin concentration in the *trans* isomer than the *cis* one. At 298 K, however, the *trans* isomer has a lower signal-to-noise ratio than the *cis* one, which suggests that more than 90% of neutral solitons undergo rapid diffusion or, in other words, during 90% of the time ratio the neutral solitons diffuse rapidly (strictly speaking, only the spin trapped for longer than $1/a_{\text{eff}}$ can contribute to the MQNMR signal). Of course, the experimental conditions should be checked carefully; they did not give any information on the spin concentration in the samples and on the accumulation number for each spectrum.

In conclusion, this experiment provides evidence for the diffuse/trap model, and may be a good quantitative test for the model if the extremely difficult quantitative analysis is successful.

5. Doped Polymers

5.1 *Polyaniline*[13,14,19]

5.1.1 *Polyaniline*

Polyaniline (PANI) is an interesting system for the following reasons. It is a stable polymer even in air, it can be oxidized with several protonic acids while keeping the electron number on the chain constant and it has relatively high electrical conductivity of up to several hundred S/cm.[1,57,58] Very recently, up to several thousand S/cm was achieved in highly oriented and high-molecular-weight film.[59] Figure 15 shows the molecular structures for the emeraldine base (EB: unprotonated insulating form) and the emeraldine salt

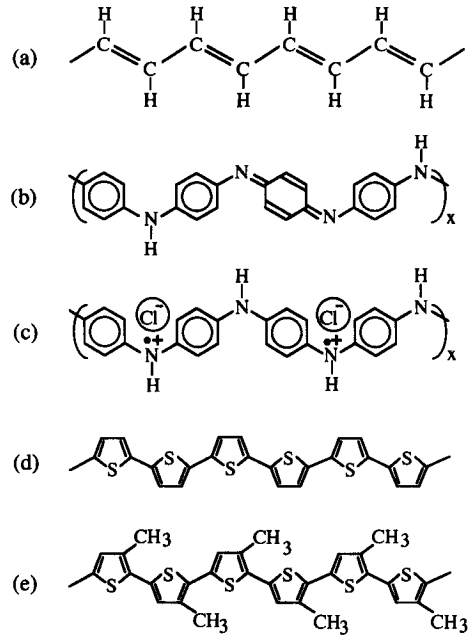

Fig. 15. The chemical structures for (a) polyacetylene, polyaniline in (b) the insulating emeraldine base (EB) form and (c) the conducting emeraldine salt (ES) form, and (d) polythiophene and (e) poly (3-methylthiophene).

(ES: protonated conducting form). An intermediate level of protonation could be achieved by dipping them in hydrochloric acid of an appropriate pH. The protonation induces some changes of the physical properties; the electrical conductivity varies from 10^{-9} (pH $\geq$ 7) to more than 10 S/cm (pH = 0),[60] and the magnetic susceptibility increases by more than two orders of magnitude, where the Pauli-like temperature-independent term is found to be proportional to the protonation level in powder form.[61] This implies a percolation transition with highly protonated conducting islands. Concerning the nature of the conducting state, two models have been proposed: Fermi glass resulting from heavy disorder by amino functions,[62] and polaronic metal.[61]

PANI has been reported to have two different crystal structures for each form: EB-I, II and ES-I, II. As synthesized powder has the structure ES-I and can be converted to unprotonated EB-I. Stretch-aligned film cast from N-methylpyrrolidinone (NMP) solution of PANI has the other structure of EB-II and its protonated form of ES-II. EB-I is amorphous and other forms have up to 50% of crystallinity.[63] In this section, we will discuss the spin dynamics of the powder samples, EB-I and ES-I, and their intermediates protonated by HCl, studied mainly in collaboration with a group located in Grenoble, France.[13,14,62,64,65]

5.1.2 *Protonation dependence of diffusion rate*[13]

As the first step, the frequency dependence of the proton NMR has been measured. In proton NMR T_1^{-1}, two different spectral densities $\phi(\omega_n)$ and $\phi(\omega_e)$ appear in a relaxation formula similar to eq. (2.11).[9] Since ω_e is more than 600 times larger than ω_n, we can observe only one of them. However, it is hard to distinguish which one of them is observed. In such a case ESR is a

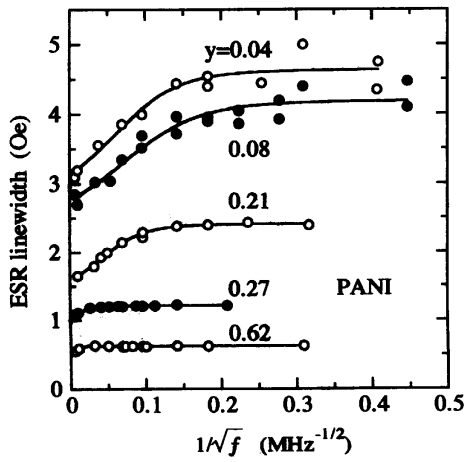

Fig. 16. The frequency dependence of ESR linewidth with implicit parameter of the protonation level y. Solid curves indicate sum of the behavior expected from eq. (2.11) for Q1D diffusion and a constant as a fitting parameter. The slope of linear increase is proportional to $1/\sqrt{D_{//}}$, and the frequency where the linewidth levels off corresponds to $D_\perp$.

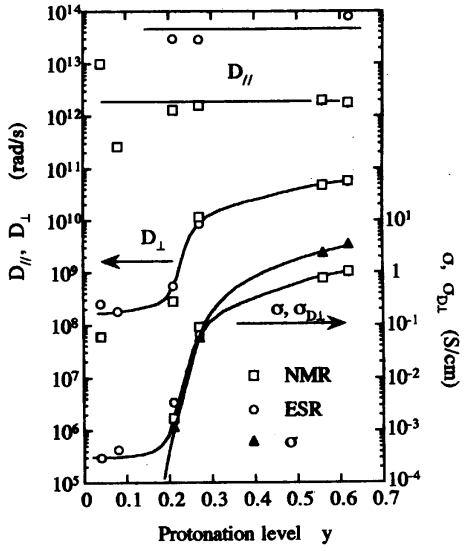

Fig. 17. The protonation level dependence of the diffusion rates $D_{//}$ along and $D_\perp$ across the chains, together with the dc electrical conductivity σ and the microscopic conductivity $\sigma_{D_\perp}$. Note the small dependence of $D_{//}$ on y and the similarity of $\sigma_{D_\perp}$ to σ.

useful method, because eq. (2.11) includes only $\phi(\omega_e)$.

Figure 16 shows the frequency dependence of the ESR linewidth for the samples with five different protonation levels. Some characteristic features appeared with increasing protonation level y: (1) the linewidth markedly decreases, and (2) the cutoff frequency $D_\perp$ increases. The linewidth also includes an excess constant contribution, as in the case of polyacetylene, but it is different from the width due to trapping in *trans*-polyacetylene, in the fact that the whole observed width in PANI comes from the relaxation, i.e., $T_1^{-1}=T_2^{*-1}$ (=the linewidth) at the plateau region,[64] in contrast with $T_1^{-1}=T_2^{*-1}-\Delta H_{\text{trap}}$ in polyacetylene. Therefore, the linewidth in PANI must result from relaxation mechanisms other than trapping, for example, interaction with absorbed oxygen which is known to broaden the ESR linewidth considerably.[62,66]

The protonation dependence for $D_{//}$ and $D_\perp$ is shown in Fig. 17, together with that of the dc electrical conductivity σ. Here, $\Sigma_l=3.2\times10^{45}$ cm^{-6} is used based on the structure proposed by Pouget *et al.*[63] This figure for Σ_l is larger than in the former report,[13] which is the reason why the present $D_{//}$ by ESR is larger than in the former report and that by NMR. A possible origin of this discrepancy between ESR and NMR is the underestimation of the hyperfine coupling constant for NMR with the electron spin.

There are some interesting features in this figure: (1) $D_{//}$ shows no definite dependence on y, (2) $D_\perp$ shows a steep change around $y=0.2$–0.3 and (3) the microscopic conductivity $\sigma_{D_\perp}$ behaves quite similarly to the dc conductivity. From these features, we can conclude that Fig. 17 shows microscopic evidence of the percolation transition of the well-protonated chains and that the dc conductivity is limited by the interchain hopping rate $D_\perp$.[13,14,64]

The reason is as follows. The first feature suggests that all the spins produced by protonation have an approximately constant diffusion rate $D_{//}$ independent of the protonation level y. This can be accounted for by assuming that such chains with the observed spins are fully protonated, irrespective of y. The second feature indicates that the spins in the fully protonated chains easily hop to the neighboring chains around $y=0.2$–0.3, where such protonated chains are probably connected to each other, that is, this is the percolation transition observed microscopically. Related to this, the third feature demonstrates that the dc conductivity is limited by the conduction $\sigma_{D_\perp}$ through the interchain diffusion $D_\perp$. This conclusion is reconfirmed in the case of the temperature dependence of $D_\perp$,[14,65] as will be discussed in the next section.

For the second feature, another interpretation that the steep change of $D_\perp$ resulted from a change of the lattice constant observed by X-ray analysis[63] has been proposed.[67] This is an interesting idea, but most of the change in the lattice constant is accomplished below $y\approx0.2$; there actually is no change between $y=0.2$ and 0.3. As is seen in Fig. 17, however, a change of σ and $D_\perp$ by two orders of magnitude occurs between $y=0.2$ and 0.3. Therefore, it is hard to assign the change of the lattice constant as an origin of this steep change in $D_\perp$.

It is found that below $y=0.2$ $D_\perp$ levels off around 10^8 rad/s. This can be understood to be bottlenecked by a mechanism other than interchain hopping (i.e. $D_\perp<\tau_\perp^{-1}$), for example, exchange coupling[46] or the finite chain length effect discussed in §2.5. $D_\perp$ itself is expected to steeply decrease further.

The microscopic conductivity $\sigma_{D_\perp}$ at 300 K is estimated as ≈1 S/cm. Here, the relation $\sigma_{D_\perp}=e^2N(E_F)D_\perp c_\perp^2$ for a metal is used, because a metallic temperature dependence for $D_{//}$ will be obtained in the next section. This value is somewhat lower than the measured dc conductivity 3.5 S/cm, but is consistent with the

presence of the parallel diffusion path through $D_{//}$. The dc conduction limited by $D_{\perp}$ suggests a presence of heavy local disorder like tangled wires. In such a case, stretch alignment may strongly enhance the conductivity, but unfortunately, it will still be limited by $D_{\perp}$ conduction, as was found experimentally.[57]

5.1.3 *Temperature dependence of diffusion rate*[14,19]

Figures 18(a) and 18(b) show the frequency dependence of the ESR linewidth for the most protonated PANI powder, with an implicit parameter of temperature above and below 150 K, respectively.[14] It is noted that the initial slope proportional to $1/\sqrt{D_{//}}$ increases both above and below 150 K, and the cutoff frequency $D_{\perp}$ decreases monotonically with decreasing temperature. The solid curves exhibit the expected behavior of eq. (2.11) obtained by least squares fitting. The obtained parameters $D_{//}$ and $D_{\perp}$ are shown in Fig. 19 as a function of the temperature, together with the dc conductivity σ for the same sample.

The characteristic features are as follows.

(1) The metallic temperature dependence of $D_{//}$ is proportional to T^{-d} with $d=2$–3 above 150 K, but semiconducting for $D_{\perp}$.

(2) The anisotropy ratio $D_{//}/D_{\perp}$ is larger than 10^5 around 150 K.

(3) There is an abrupt change in $D_{//}$ around 150 K.

(4) The proportionality of $D_{\perp}$ to dc conductivity σ holds down to 120 K.

(1) and (2) are clear evidence that PANI-HCl is a Q1D metal above 150 K. The possibility of a 1D metal has been discussed theoretically by some authors.[68,69] The present conclusion of the Q1D metal is interesting compared to that in which the stretch-aligned PANI-ES-II film is a 3D metal, deduced from the thermoelectric power S and the dielectric constant ε.[57,70] A possible origin of this difference could be the structural difference between the ES-I powder studied here and ES-II film. Very recently, the importance of controlling the local structural order was demonstrated in realizing 3D metallic film.[71] Presently, the spin dynamics study on ES-II film is in progress to clarify this difference in PANI-HCl. The order of the power law $d=2$–3 in $D_{//}$ is difficult to determine with higher accuracy, because the present limit of the frequency up to 24 GHz$=2.4\times10^{10}$ Hz is not sufficiently high compared with $D_{\perp}/2\pi\approx1\times10^{10}$ Hz. Hence, at the present stage, we can only say that d is larger than two, which is a common value for many organic conductors,[72] and the VSC result of the several conducting polymers.[7]

(2) could yield the lower bound of the conjugation length of the polymer chain, as discussed in §2.5; $l_{\min}=\sqrt{D_{//}/D_{\perp}}c_{//}=\sqrt{3\times10^4}c_{//}=180c_{//}$ which appears reasonable considering the average molecular weight of about 50000 for PANI.[73]

The high degree of anisotropy $D_{//}/D_{\perp}=10^5$ in PANI-HCl does not contradict the observed Lorentzian line shape in ESR.[64,70] The determining factor of line shape is not the degree of anisotropy, but the condition $D_{\perp}(D_{//}/D_{\perp})^{1/4}\gg\sqrt{\langle\omega^2\rangle}=9.4\times10^8$ rad/s, where $\langle\omega^2\rangle$ is the second moment of the dipolar interaction between the electron spins.[51,74] In the present case, $D_{\perp}(D_{//}/D_{\perp})^{1/4}\geq10^{10}$ rad/s is large enough to satisfy the above condition at all temperatures. Therefore, the Lorentzian line shape is a reasonable observation in PANI-HCl, and is consistent with the high anisotropy ratio.

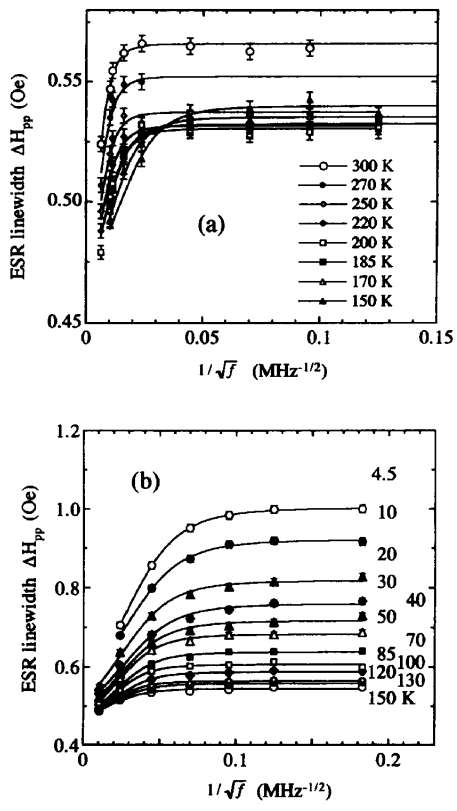

Fig. 18. The frequency dependence of ESR linewidth with an implicit parameter of temperature (a) above and (b) below 150 K. Anomaly of the slope at 150 K can be found by noting that the slope increases with both increasing and decreasing temperature from 150 K.

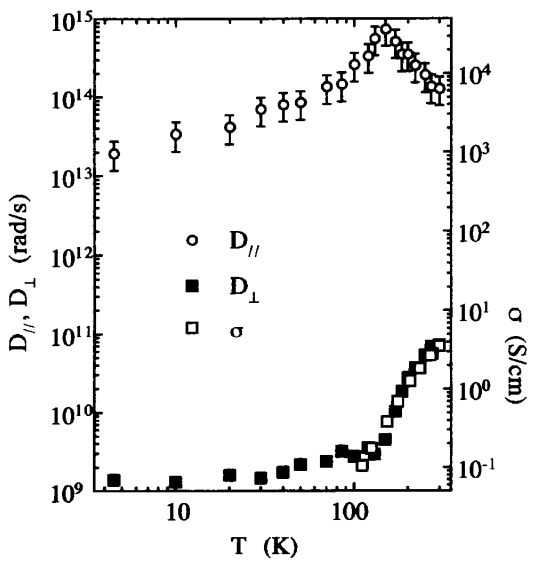

Fig. 19. The temperature dependence of the diffusion rates $D_{//}$ along and $D_{\perp}$ across the chains. Note that $D_{//}$ shows metallic temperature dependence above 150 K, and that $D_{\perp}$ is semiconducting with a temperature dependence similar to that of σ.

The microscopic conductivity along the chain $\sigma_{D_{/\!/}}$ can be estimated as 1.5×10^3 S/cm at 300 K from the relation $\sigma_{D_{/\!/}}=e^2N(E_F)D_{/\!/}c_{/\!/}^2$, which is interesting in comparison with the recent estimation of σ for PANI-CSA film.[75] The mean free path l^* can also be estimated as $0.5c_{/\!/}$ at 300 K and $5c_{/\!/}$ at 150 K.[14,19] These values suggest that PANI-HCl is in the boundary between metals and electron localization.

(3) suggests a phase change at 150 K from semiconductor to metal. This temperature is close to the minimum temperature of the thermoelectric power S for the ES-I powder.[57] Since this minimum shifts to lower temperature with increasing crystallinity, the phase change is related to the crystallinity of the sample. Preliminary data of the spin dynamics show that with decreasing y the temperature of phase change increases,[19] which suggests a suppression of the phase change by the three-dimensional interaction increased by protonation. The temperature dependence below 150 K is somewhat curious. Although $1/D_{/\!/}\propto\log T$, $D_{/\!/}\propto\sqrt{T}$ or $D_{/\!/}\propto\exp\{bT\}$ apparently holds within a large error range, applicability of these formulae is not clear when absolute magnitudes are included.[14] These dependences are also found in PANI-H_2SO_4.[76] The physical meaning of the temperature dependence below 150 K remains to be solved.

5.2 *Polythiophene, Poly(3-methylthiophene)*[15,18]

5.2.1 *Materials*

The ESR experiment on polythiophene (PT) and poly(3-methylthiophene) (PMT) with ClO_4 (-Cl) and PF_6 (-PF) as dopants have been performed with the parameters of temperature and frequency,[15,18] and will be briefly reviewed here. The chemical formulae of these polymers are shown in Fig. 15. The samples were prepared by electrochemical polymerization.[77]

A characteristic feature in these materials is that both the spin diffusion and the Elliott mechanism[78] dominate the ESR linewidth. The former was observed from frequency dependence and the latter from temperature dependence. Analysis of these data provides the possibility of deducing many electronic structures related to the anisotropic diffusion rates $D_{/\!/}$ and $D_\perp$, the relaxation time $\tau_{/\!/}$ of resistivity, the Fermi velocity $V_{F_{/\!/}}$, the mean free path l^* and the anisotropic electrical conductivities $\sigma_{/\!/}$ and $\sigma_\perp$.

5.2.2 *Frequency dependence of ESR linewidth*

Figure 20 shows the frequency dependence of the ESR linewidth that starts to decrease above 1 GHz and shows steep increase above 8.5 GHz. This curious behavior is understandable in terms of an extra broadening due to anisotropy of g-shift. In the polycrystalline materials, the anisotropy of g-shift cannot be resolved, but is distributed to broaden the ESR linewidth. Such a width due to the g-shift should be proportional to the external magnetic field strength. The solid curve is a least squares fit to a sum of the three terms contributing to the observed linewidth: the Elliott, the Q1D diffusive motion and the anisotropy of g-shift. Here, $D_{/\!/}$ and $D_\perp$ were obtained as fitting parameters. This fitting reproduces the data fairly well with the Q1D diffusion, in spite of the 3D anisotropic structure determined for the polypyrrole[79] and poly(3-alkylthiophene)s[80,81] that have structures similar to PT. If this is the case, one expects the two-dimensional regime where $J(\omega)\propto\log\omega$. The actual system, however, shows approximate Q1D behavior, indicating that the electronic state of this polymer is still a good Q1D. A probable reason is that the crystallinity is low enough to isolate the chains.

Finally, we obtained $D_{/\!/}=1.9\times10^{15}$ rad/s and $D_\perp=5.5\times10^9$ rad/s with the lattice parameters, $a=3.65$ Å, $b=12.5$ Å and $c=3.9$ Å, and $N(E_F)=0.47$ states/(eV·ring) for both spin directions estimated from the Pauli susceptibility χ_P obtained by the Schumacher-Slichter method.[82] Thus the obtained diffusion rates and the density of states give an estimate of the microscopic conductivity as $\sigma_{D_{/\!/}}=1.2\times10^3$ S/cm and $\sigma_{D_\perp}=3.7\times10^{-2}$ S/cm at 300 K. The observed $\sigma_{dc}=150$ S/cm is compatible with these values, since $\sigma_{D_\perp}=3.7\times10^{-2}$ S/cm forms a network with $\sigma_{D_{/\!/}}=1.2\times10^3$ S/cm. Here, note that the absolute value of $\sigma_{D_{/\!/}}$ should be regarded with caution, since $\sigma_{D_{/\!/}}$ depends greatly on $N(E_F)^3$ and ΣI^2.

5.2.3 *Temperature dependence of ESR linewidth*

The temperature dependence of the ESR linewidth for PT-Cl and PMT-Cl are shown in Fig. 21. It is noted that both of the linewidths increase with increasing temperature, similarly to metallic resistivity. This be-

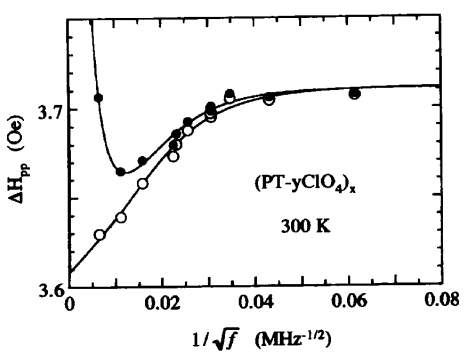

Fig. 20. The frequency dependence of ESR linewidth for PT-ClO_4^- at 300 K. The closed circles show the raw data and the open circles are linewidths corrected by the g-anisotropy broadening which is proportional to the external magnetic field strength.

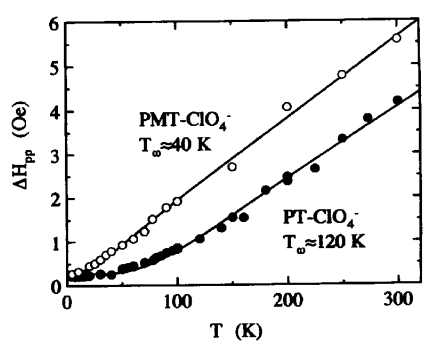

Fig. 21. The temperature dependence of ESR linewidth for PT-ClO_4^- and PMT-ClO_4^- measured at 50 MHz. Note the qualitative difference in the temperature dependences for the two materials. The solid curves show the qualitative predictions of eq. (5.2) with T_ω's shown in the figure.

havior is consistent with the reported data.[83,84] More careful inspection reveals a difference in their temperature dependence as linear for PMT-Cl and approximately quadratic for PT-Cl.[15,18,77] Interestingly, the temperature dependence of the VSC resistance has been found to show a similar tendency to that of the linewidth.[18,85] This is particularly pronounced when the ESR linewidth is governed by the Elliott mechanism[78] through scattering via spin-orbit interaction.

If this is the case, one can try to estimate the scattering lifetime τ_s with spin-flips as $\tau_s=2/(\sqrt{3}\gamma_s\Delta H_{pp}) \approx 1.8\times10^{-8}$ s from the observed linewidth $\Delta H_{pp}=3.7$ Oe. Using τ_s, one obtains the scattering relaxation time $\tau_{/\!/}=\tau_s(\Delta g)^2/\alpha$ for the resistivity, where Δg is the ESR g-shift and α is the constant that should be estimated theoretically or experimentally.[78] In the case of typical Q1D-system TTF-TCNQ, a relationship $\alpha\approx\tau_\perp/\tau_{/\!/}$ was found.[86] If this is applied to the present case with $\alpha=2.9\times10^{-6}$ and $\Delta g=3.8\times10^{-4}$, *a priori* incorrect value $\tau_{/\!/}=8.9\times10^{-10}$ s is obtained, which surprisingly yields $\sigma\approx4\times10^8$ S/cm with $\sigma=ne^2\tau_{/\!/}/m_0$. Here, n is the carrier concentration and m_0 is the free electron mass. This shows inapplicability of the relationship $\alpha\approx\tau_\perp/\tau_{/\!/}$ to conducting polymers. Furthermore, no definite correlation between g-shift and ΔH was found in conducting polymers, irrespective of a good correlation between ΔH and the fourth power of atomic numbers of the heaviest atom.[18] These findings suggest that the g-shift in conducting polymers is governed by molecular symmetry of monomer molecule, instead of size of the spin-orbit splitting in metallic band.[78] Therefore, quantitative analysis with the Elliott mechanism in conducting polymers is a problem to be solved by future investigation.

5.2.4 *Parameters for electronic states*

If one assumes a 1D metal as a good approximation for PT, the Fermi velocity can be estimated as $V_{F/\!/}=2L/(\pi\hbar N(E_F))=8.0\times10^7$ cm/s with $N(E_F)=0.47$ states/(eV·ring). Then, the mean free path, $l^*=D_{/\!/}c_{/\!/}^2/V_{F/\!/}$, of conduction electron is obtained to be $\approx c_{/\!/}$. Consequently, $\tau_{/\!/}\approx5\times10^{-16}$ s is derived from the relation $l^*=V_{F/\!/}\tau_{/\!/}\approx c_{/\!/}$. This scattering relaxation time predicts with $\tau_{/\!/}=\tau_s(\Delta g)^2/\alpha$ that α is an order of unity, similarly to alkali metals.[87] This conclusion markedly differs from in TTF-TCNQ. The parameters obtained for the electronic states in PT are summarized in Table III.

Anisotropy of conductivity is very large, greater than 10^4 at 300 K. This large value can be compared with 10^3–10^5 for the PANI-HCl powder. These findings demonstrate that these polymers are good Q1D metals.

Table III. The parameters for polythiophene obtained at 300 K from the analysis of ESR broadening by the diffusion and the Elliott mechanism. D is the diffusion rate, τ the relaxation time for scattering, V_F the Fermi velocity, l^* the mean free path and σ the electrical conductivity.

	D (rad/s)	τ (s)	V_F (cm/s)	l^* ($c_{/\!/}$ or $c_\perp$)	σ (S/cm)
//	1.9×10^{15}	5×10^{-16}	8.0×10^7	≈1	1.2×10^3
⊥	5.5×10^9				0.037

However, it must be noted that they are severely disordered materials and it will be very interesting to study the systems with highly ordered structure. Finally, the minimum conjugation length is given by $l_{min}=\sqrt{D_{/\!/}/D_\perp}c_{/\!/}=580c_{/\!/}$.

In conclusion the temperature and frequency dependences of the ESR linewidth are consistently understandable in terms of the contribution of the conduction electon spins, and suggest that the temperature dependence of the resistivity is quadratic for PT-Cl in the entire temperature range, but is T-linear for PMT-Cl, and becomes quadratic below 30 K.[15,18]

5.3 *Polyacetylene*[26,27]

5.3.1 *^{1}H NMR study in heavily doped polyacetylene*

In this section spin dynamics studied with NMR will be reviewed.

In 1980, the spin dynamics study of heavily doped polyacetylene was reported for AsF_5-doped $(CH)_x$ at room temperature by Nechtschein *et al.*,[25] and it was concluded that the microscopic conductivity along the chain was higher than 10^4 S/cm. Unfortunately, this conclusion is ambiguous in that the observed relaxation can be understood not only in terms of the metallic electrons but also in terms of the neutral solitons remaining in the doped sample. At that stage, the estimated microscopic conductivity was not clarified even at 300 K, to say nothing of temperature dependence, but was known only to be minimum. To confirm this, various contributions to the relaxation rate must be discriminated, especially as a function of temperature. Therefore, a systematic study on heavily doped polyacetylene with several dopant species with NMR T_1^{-1} was carried out.[26,27]

In most kinds of conducting polymers, both the Curie and the Pauli susceptibilities have been observed.[88] The Pauli susceptibility is understood in terms of the conduction electrons. The Curie one may be concerned with polarons in short conjugation chains, but is not yet well defined. Figure 22 shows a good correlation between NMR T_1^{-1} and the number of Curie spins in FSO_3^-, ClO_4^-, I_3^-, Br_3^- and K^+-doped[89] polyacetylenes both (a) at 9 K and 15 MHz, and (b) at 20 K and 50.5 MHz. This well-defined correlation suggests that NMR T_1^{-1} is dominated by the Curie spins in these doped polyacetylenes at least in such a low temperature

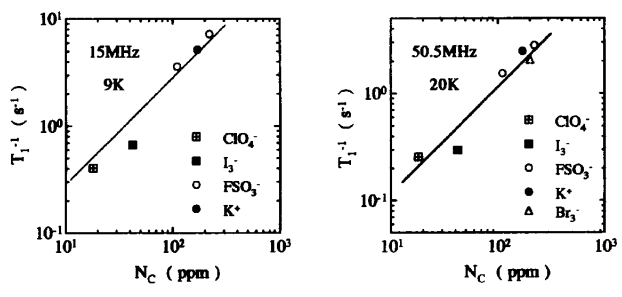

Fig. 22. NMR T_1^{-1} as a function of the number of Curie spins measured by both SQUID susceptometer and Schumacher-Slichter method in the polyacetylene heavily doped with several different species. (a) 9 K and 15 MHz (b) 20 K and 50.5 MHz

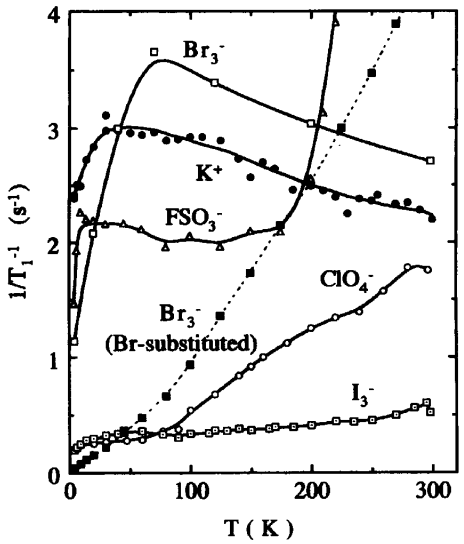

Fig. 23. The typical temperature dependence of NMR T_1^{-1} measured at 50 MHz in K^+, Br_3^-, I_3^-, ClO_4^-, and FSO_3^--doped $(CH)_x$.[26,27,90,91] The steep increase around 200 K in the case of FSO_3^- is due to molecular motion, as probably is the gradual increase in the case of ClO_4^-. The solid curves are guides for the eyes.

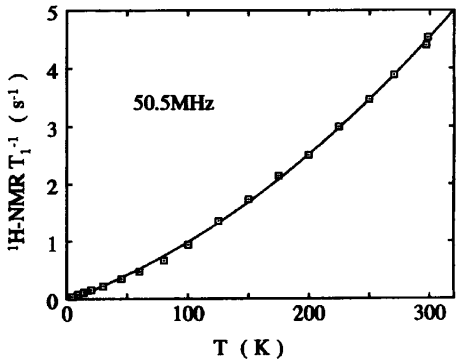

Fig. 24. The temperature dependence of NMR T_1^{-1} in Br_3-doped $(CH_{1-y}Br_y)_x$. It is noted that the temperature dependence is steeper than T_1T=const.

region. In the higher temperature range, this kind of correlation breaks down because of the appearance of other relaxation mechanisms such as molecular motion and metallic relaxation. The typical temperature dependences of NMR T_1^{-1} are shown in Fig. 23,[26,27,90,91] which is a familiar temperature dependence found in many other conducting polymers, for example, polythiophene,[92] polypyrrole[93] and polyaniline.[94]

Although the origin of the Curie spins has not been established yet,[95] it should be noted that the NMR T_1^{-1} could not be used to study the spin dynamics in these cases, which is in contrast to the ESR case discussed in §5.1 and §5.2. One possible origin of the Curie spins is a neutral soliton confined in a limited area.[36] In the systems with a low number of Curie spins, for example in I_3^--doped $(CH)_x$, metallic contribution to NMR T_1^{-1}, in addition to that due to the Curie spins, seems to be observed in the higher temperature range. The reasons why metallic NMR T_1^{-1} is difficult to observe are that (1) the higher the conductivity, the smaller the relaxation rate and (2) NMR T_1^{-1} is easily affected by the molecular motions of chain and/or dopant molecules, and by the localized electron spins. Then, if one can control the conductivity and the Curie spin contribution, it becomes possible to study the spin dynamics in conducting polymers. Such an example was found in the polyacetylene modified by substituting Br for proton.[26,27,96] Such a modification was demonstrated for the first time by Kletter *et al.*[97]

5.3.2 *Temperature dependence of microscopic conductivity*

Br_3^--doped polyacetylene shows a typical temperature dependence of the relaxation rate dominated by the Curie spin.[26,27] It was found, however, that in some Br_3^--doped cases NMR T_1^{-1} showed a characteristic behavior in 3D metals, T_1T=const.[96] It has been revealed by a systematic study of this system that the different behavior of NMR T_1^{-1} resulted from a difference in the Br substitution level.[26,27] The higher the Br-substitution, the steeper the temperature dependence of NMR T_1^{-1} than T_1T=const., as typically shown in Fig. 24. This superlinear law in T_1T^n=const. is an expected temperature variation in low-dimensional metallic systems carrying Pauli susceptibility, for example,

$$T_1T/\sqrt{D_{//}}=T_1T^{3/2}=\text{const.}, \tag{5.1}$$

derived from eq. (2.10) for the case of $\sigma \propto D_{//} \propto 1/T$. Several possible reasons why the metallic relaxation was observed successfully in this system may be that (1) the random potential produced by the Br substitution induced the scattering of the electrons, (2) the phonon scattering of the electrons was enhanced by an increase of the number of phonons of which energy was lowered by the seventy-times-heavier mass of the Br atom than the proton, and (3) the relaxation centers of the diffusing Curie spins were deactivated because of a confinement due to the random potential.

Figure 25 shows the temperature dependence of the microscopic resistivity deduced from Fig. 24. The room-temperature resistivity is on the order of $3\times10^{-4}\,\Omega\cdot$cm which is much smaller than the $\sim$0.1 $\Omega\cdot$cm for the dc conductivity, but is considerably large compared with the less than $10^{-5}\,\Omega\cdot$cm obtained in the iodine-doped Naarmann-type polyacetylene,[27,48,49] probably because of the randomness introduced by the Br substitution. Although the scattering of the data is fairly large at low temperature, the characteristic power law behavior was found; $\rho \propto T$ at temperatures higher than 100 K and ρ approaches T^2 below 100 K. This behavior can be understood in terms of the phonon and impurity scattering similar to those in the usual 3D metallic systems, but disagrees with the theoretical prediction of $\rho \propto \exp\{T/T_a\}$ for the Q1D metals in the low-temperature limit $T \ll T_a$, where T_a is the characteristic temperature larger than 1000 K.[98] A similar conclusion on the temperature dependence of the resistivity has been found in many systems with the dopants I_3^-, ClO_4^-, FSO_3^- and $FeCl_4^-$, by the VSC technique.[7,99] If a 1D metal without the restriction $T \ll T_a$ applied in

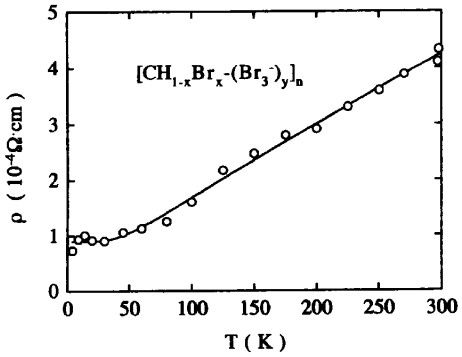

Fig. 25. The temperature dependence of the microscopic resistivity $\rho_{//}$ in Br_3-doped $(CH_{1-y}Br_y)_x$. The solid curve is the prediction for 1D metal described by eq. (5.2) with $\hbar\omega_0/k_B=160$ K.

ref. 98 is assumed, the resistivity due to single phonon scattering is[26,27]

$$\rho_{ph}=\frac{\pi^2\hbar\Sigma}{e^2}\frac{\alpha^2 D(E_F)}{M\omega_0 V_F}\frac{1}{\cosh(\hbar\omega_0/2k_BT)\sinh(\hbar\omega_0/2k_BT)}, \tag{5.2}$$

where Σ is the cross-sectional area for a single chain, α the electron phonon coupling constant and ω_0 the phonon frequency with $q=2k_F$ causing carrier scattering in the 1D electronic systems; the other symbols have their usual meanings. The sum of eq. (5.2) with $\hbar\omega_0/k_B=160$ K and a constant residual resistivity can reproduce the data well, as shown by the solid curve in Fig. 25. It has also been reported that eq. (5.2) with $\hbar\omega_0/k_B=40$–120 K could reproduce the temperature dependence of the ESR linewidth dominated by the Elliott mechanism (the solid curves in Fig. 21) and R_{VSC} for poly-thiophene and poly(3-methylthiophene) doped by ClO_4^- and AsF_6^-.[18] These results suggest that the metallic state in the doped polymers is normal metal state.

Finally, the minimum conductivity expected from the NMR relaxation data is discussed. T_1^{-1} is definitely dominated by the Curie spin contribution, at least at low temperatures. However, since the Curie contribution changes little with temperature and the metallic one increases with increasing temperature, T_1^{-1} yields the minimum conductivity normalized by the Br-substituted case around 300 K: $\rho_{//}\leq 5\times10^{-6}\,\Omega\cdot$cm for the I_3^- case and $\rho_{//}\leq 5\times10^{-5}\,\Omega\cdot$cm for the ClO_4^- case. In the ClO_4^- case, the obtained value is overestimated compared to in the I_3^- case, because the ClO_4^- ion provides additional relaxation due to molecular rotation. These values agree with the recently observed dc conductivities.[5,27,48,49]

6. Comparison of ESR with NMR in Spin Dynamics Study

In the preceding sections we reviewed spin dynamics studied by ESR and NMR. The apparent behaviors of ESR and NMR are similar in some cases but contradictory in other cases. Neutral soliton dynamics studies in pristine *t*-polyacetylene have led to the conclusion that both of the techniques revealed the same physics and were complementary methods for the study of spin dynamics (§4).[7-12,23-25]

In the doped conducting polymers, however, circumstances are different. As shown in §5.1 and 5.2, ESR linewidth seems to reflect the carrier spin dynamics and could be analyzed to give information on the microscopic conductivity; in some cases it is metallic and in other cases it is semiconducting. Especially in polythiophenes, not only the diffusive motion, but also the Elliott mechanism helps us to obtain information on the electronic structures of the conducting polymers. In the ESR study, a small number of localized spins do not contribute to the Elliott mechanism but simply act as spins diffusing with $D_{//}$ instead of $2D_{//}$ for the mutually diffusing spins. On the other hand, NMR also detects relaxation mechanisms other than diffusive motion, for example, relaxation to nearly localized paramagnetic spins and molecular motions. The nearly localized Curie-spin concentration down to 20 ppm is sufficiently high to mask the temperature variation of NMR relaxation due to the conduction electron spins. It is considered that this is the reason why proton NMR relaxation in many conducting polymers show similar temperature dependence and never indicate metallic behavior after analysis in terms of diffusive motion, even in systems where metallic indications have been observed by other experimental methods such as thermoelectric power, optical absorption and dc electrical conductivity at temperatures higher than 200 K.

In the example of Br substitution in polyacetylene, the above-mentioned barrier was overcome and the temperature dependence of the microscopic resistivity was elucidated in order to discuss the electronic structure in this polymer (§5.3). Generally speaking, NMR has two pick-up windows in different frequency ranges, ω_e and ω_n, differing by ~670 times. This is extremely important for effective survey of a wide frequency range. Therefore, if the above-mentioned barrier is removed to study the spin dynamics, NMR and ESR are in fact complementary techniques.

7. Concluding Remarks

It has been ten years, since the first ESR study as a function of frequency was applied to neutral soliton dynamics in polyacetylene. During this period the relaxation mechanism has been confirmed through the concentration dependence and the anisotropic behavior in stretch aligned film. Furthermore, the temperature dependence of the diffusion rate in polyacetylene has been studied. Subsequently, the conducting state of polyaniline was investigated in Grenoble in collaboration with Dr. M. Nechtschein, and the percolation transition as a function of the protonation level was revealed. The diffusion rate along the chain in the conducting polymer could be studied by modifying the spectrometer into a frequency variable up to K-band (24 GHz). For PANI and PT, the study of diffusion rates along the chain has recently become possible.

One of the interesting aims in spin dynamics study is to clarify the microscopic conductivity in doped poly-

acetylene. Our many efforts to reveal it by the NMR technique have failed because of the reasons mentioned in §5.3. Recently, however, successful analysis of the microscopic conductivity in a system analogous to doped polyacetylene, $[(CH_{1-\delta}Br_{\delta})-(Br_3^-)_y]_x$, where relaxation mechanisms other than diffusive motion were suppressed because of the introduction of random potentials by Br-substitution, was achieved. The obtained temperature dependence of the microscopic conductivity is normal; i.e., it shows the residual resistivity due to random potentials and that due to phonon scattering following a T-linear law at high temperatures.

From the viewpoint of clarifying the intrinsic transport properties, it is also interesting to note that the VSC results obtained have shown a temperature dependence of the resistance consistent with the spin dynamics results presented here for several conducting polymers. The recently obtained thermoelectric power data indicate a metal-semiconductor transition around 10 K in PT and well below 10 K in PMT metallic samples.[77,85] We expect an ability for the spin dynamics to investigate such phase transitions. There are other unresolved issues to be studied further concerning well-characterized, stretch-aligned and well-crystallized conducting polymers.

Acknowledgments

The author would like to express his sincere thanks to Dr. M. Nechtschein and Dr. J.-P. Travers for their collaboration and exciting and useful discussions on the work on polyaniline, and to Dr. F. Shimizu, Mr. M. Honda, Dr. S. Masubuchi, and Professors S. Kasama, H. Shirakawa, Y. Onodera and K. Kume for their collaboration and stimulating discussions on polyacetylenes and poly(3-alkylthiophene)s. He also thanks to Professor J. Isoya for offering unpublished data on T_M. This work is partly supported by a Grant-in-Aid for Scientific Research (C) from the Ministry of Education, Science and Culture (No. 03640321).

1) See, for example, *Proc. Int. Conf. Science and Technology of Synthetic Metals (ICSM'92), Göteborg, 1992*, Synth. Met. **55–57** (1993).
2) As a review, see *Conjugated Conducting Polymers*, ed. H. Kiess (Springer-Verlag, Berlin, 1992).
3) P. Sheng: Phys. Rev. B **21** (1980) 2180.
4) N. F. Mott and E. A. Davis: *Electronic Processes in Noncrystalline Materials* (Clarendon Press, Oxford, 1979) 2nd ed.
5) S. Masubuchi, S. Kazama, K. Mizoguchi, F. Shimizu, K. Kume, R. Matsushita and T. Matsuyama: Synth. Met. **55–57** (1993) 4866.
6) A. B. Kaiser: Synth. Met. **45** (1991) 183.
7) S. Masubuchi, K. Mizoguchi, K. Mizuno and K. Kume: Synth. Met. **22** (1987) 41.
8) K. Mizoguchi, K. Kume and H. Shirakawa: Solid State Commun. **50** (1984) 213.
9) K. Mizoguchi: Makromol. Chem., Macromol. Symp. **37** (1990) 53.
10) K. Mizoguchi, K. Kume, S. Masubuchi and H. Shirakawa: Solid State Commun. **59** (1986) 465.
11) K. Mizoguchi, K. Kume and H. Shirakawa: Synth. Met. **17** (1987) 439.
12) K. Mizoguchi, S. Komukai, T. Tsukamoto, K. Kume. M. Suezaki, K. Akagi and H. Shirakawa: Synth. Met. **28** (1989) D393.
13) K. Mizoguchi, M. Nechtschein, J.-P. Travers and C. Menardo: Phys. Rev. Lett. **63** (1989) 66.
14) K. Mizoguchi and K. Kume: Solid State Commun. **89** (1994) 971.
15) K. Mizoguchi, M. Honda, S. Masubuchi, S. Kazama and K. Kume: Jpn. J. Appl. Phys. **33** (1994) L1239.
16) K. Mizoguchi, H. Sakurai, F. Shimizu, S. Masubuchi and K. Kume: to be published in Synth. Met.
17) K. Mizoguchi, S. Masubuchi, K. Kume, K. Akagi and H. Shirakawa: submitted to Phys. Rev. B.
18) K. Mizoguchi, M. Honda, F. Shimizu, S. Masubuchi, S. Kazama, H. Sakamoto and K. Kume: in preparation for publication.
19) K. Mizoguchi and K. Kume: *Proc. Int. Conf. Science and Technology of Synthetic Metals (ICSM'94), Seoul, 1994*, to be published in Synth. Met.
20) K. Mizoguchi, H. Sakurai, F. Shimizu, S. Masubuchi and K. Kume: *Proc. Int. Conf. Science and Technology of Synthetic Metals (ICSM'94), Seoul, 1994*, to be published in Synth. Met.
21) For example, G. Soda, D. Jerome, M. Weger, J. Alizon, J. Gallice, H. Robert, J. M. Fabre and L. Giral: J. Phys. (Paris) **38** (1977) 931.
22) For example, F. Devreux and M. Nechtschein: *Quasi-One-Dimensional Conductors I*, eds. S. Barisic, A. Bjelis and J. Copper (Springer-Verlag, New York, 1979) Lecture Notes in Physics, Vol. 95, p. 145.
23) M. Nechtschein, F. Devreux, R. L. Greene, T. C. Clarke and G. B. Street: Phys. Rev. Lett. **44** (1980) 356.
24) K. Holczer, J. P. Boucher, F. Devreux and M. Nechtschein: Phys. Rev. B **26** (1981) 1051.
25) M. Nechtschein, F. Devreux, F. Genoud, M. Guglielmi and K. Holczer: Phys. Rev. B **27** (1983) 61.
26) F. Shimizu: PhD. Thesis, Faculty of Science, Tokyo Metropolitan University, Tokyo, 1994.
27) F. Shimizu, K. Mizoguchi, S. Masubuchi and K. Kume: *Proc. Int. Conf. Science and Technology of Synthetic Metals (ICSM'94), Seoul, 1994*, to be published in Synth. Met.
28) A. Abragam: *Principles of Nuclear Magnetism* (Oxford University, Oxford, 1961) Chap. 8.
29) C. A. Sholl: J. Phys. C **14** (1981) 447.
30) M. A. Butler, L. R. Walker and Z. G. Soos: J. Chem. Phys. **64** (1976) 3592.
31) P. C. Stein and P. Bernier: Phys. Rev. B **37** (1988) 10637.
32) F. Devreux: Phys. Rev. B **25** (1982) 6609.
33) W. P. Su, J. R. Schrieffer and A. J. Heeger: Phys. Rev. B **22** (1980) 2099.
34) K. Mizoguchi, K. Kume and H. Shirakawa: Mol. Cryst. Liq. Cryst. **118** (1985) 459.
35) W. G. Clark, K. Glover, M. D. Lan and L. J. Azevedo: J. Phys. (Paris) **44** (1983) C3-1493.
36) P. K. Kahol, M. Mehring and X. Wu: J. Phys. (Paris) **46** (1985) 163.
37) J. S. Hyde, W. Froncisz and T. Oles: J. Mag. Res. **82** (1989) 223.
38) W. G. Clark, K. Glover, G. Mozurkewich, S. Etemad and M. Maxfield: Mol. Cryst. Liq. Cryst. **117** (1985) 447.
39) S. Kuroda, M. Tokumoto, N. Kinoshita and H. Shirakawa: J. Phys. Soc. Jpn. **51** (1982) 693.
40) S. Kuroda and H. Shirakawa: Phys. Rev. B **35** (1987) 9380.
41) H. Thomann, L. R. Dalton, M. Grabowski and T. C. Clark: Phys. Rev. B **31** (1985) 3141.
42) M. Mehring, A. Grupp, P. Höfer and H. Käss: Synth. Met. **28** (1989) D399.
43) N. S. Shiren, Y. Tomkiewicz, H. Thomann, L. Dalton and T. C. Clarke: J. Phys. (Paris) **44** (1983) C3-223.
44) See for example, Y. Wada: *Nonlinear Excitations in Quasi-One-Dimensional Materials*, eds. Y. Ono, A. Terai and H. Takayama, Progr. Theor. Phys. (1993) Suppl. 113, p. 1.
45) S. Jeyadev and E. M. Conwell: Phys. Rev. B **36** (1987) 3284.

46) C. Jeandey, J. P. Boucher, F. Ferrieu and M. Nechtschein: Solid State Commun. **23** (1977) 673.
47) S. Kivelson: Phys. Rev. B **25** (1982) 3798.
48) H. Naarmann and N. Theophilou: Synth. Met. **22** (1987) 1.
49) J. Tsukamoto, A. Takahashi and K. Kawasaki: Jpn. J. Appl. Phys. **29** (1990) 125.
50) K. Akagi and H. Shirakawa: Synth. Met. **60** (1993) 85.
51) Z. H. Wang, N. Theophilou, D. B. Swanson, A. G. MacDiarmid and A. J. Epstein: Phys. Rev. B **44** (1991) 12070.
52) N. S. Shiren, Y. Tomkiewicz, T. G. Kazyaka and A. R. Taranko: Solid State Commun. **44** (1982) 1157.
53) J. Tang, C. P. Lin, M. K. Bowman, J. R. Norris, J. Isoya and H. Shirakawa: Phys. Rev. B **28** (1983) 2845.
54) B. H. Robinson, J. M. Schurr, A. L. Kwiram, H. Thomann, H. Kim, A. Morrobel-Sosa, P. Bryson and L. R. Dalton: J. Phys. Chem. **89** (1985) 4994.
55) H. Thomann, H. Jin and G. L. Baker: Phys. Rev. Lett. **59** (1987) 509.
56) J. Isoya: private communication.
57) Z. H. Wang, C. Li, E. M. Scherr, A. G. MacDiarmid and A. J. Epstein: Phys. Rev. Lett. **66** (1991) 1745.
58) A. P. Monkman and P. N. Adams: Synth. Met. **41–43** (1991) 627.
59) P. N. Adams, P. J. Laughlin A. P. Monkman and N. Bernhoeft: Solid State Commun. **91** (1994) 875.
60) A. G. MacDiarmid, J. C. Chiang, M. Halpern, W. S. Huang, S. L. Mu, N. L. D. Somasiri, W. Q. Wu and S. I. Yaniger: Mol. Cryst. Liq. Cryst. **121** (1985) 173.
61) A. G. MacDiarmid, J. C. Chiang, A. F. Richter and A. J. Epstein: Synth. Met. **18** (1987) 285.
62) M. Nechtschein, F. Genoud, C. Menardo, K. Mizoguchi, J. P. Travers and B. Villeret: Synth. Met. **29** (1989) E211.
63) J. P. Pouget, M. E. Józefowicz, A. J. Epstein, X. Tang and A. G. MacDiarmid: Macromolecules **24** (1991) 779.
64) K. Mizoguchi, M. Nechtschein, J. P. Travers and C. Menardo: Synth. Met. **29** (1989) E417.
65) K. Mizoguchi, M. Nechtschein and J. P. Travers: Synth. Met. **41** (1991) 113.
66) M. Nechtschein and F. Genoud: Solid State Commun. **91** (1994) 471.
67) A. J. Epstein, A. G. MacDiarmid and J. P. Pouget: Phys. Rev. Lett. **65** (1990) 664.
68) D. S. Galvao, D. A. dos Santos and B. Laks: Phys. Rev. Lett. **63** (1989) 786.
69) H. L. Wu and P. Phillips: Phys. Rev. Lett. **66** (1991) 1366.
70) Z. H. Wang, C. Li, E. M. Scherr, A. G. MacDiarmid and A. J. Epstein: Phys. Rev. B **45** (1992) 4190.
71) A. J. Epstein, J. Joo, R. S. Kohlman, G. Du, A. G. MacDiarmid, E. J. Oh, Y. Min, J. Tsukamoto, H. Kaneko and J. P. Pouget: Synth. Met. **65** (1994) 149.
72) For example, A. Graja: *Low-Pimensional Organic Conductors* (World Scientific, Singapore, 1992).
73) E. J. Oh, Y. Min, J. M. Wiesinger, S. K. Manohar, E. M. Scherr, P. J. Prest, A. J. MacDiarmid and A. J. Epstein: Synth. Met. **55–57** (1993) 977.
74) M. J. Hennessy, C. D. McElwee and P. M. Richards: Phys. Rev. B **7** (1973) 930.
75) M. Reghu, Y. Cao, D. Moses and A. J. Heeger: Synth. Met. **57** (1993) 5020.
76) H. K. Roth, K. Mizoguchi, M. Honda, H. Sakamoto and K. Kume: unpublished data.
77) S. Masubuchi, S. Kazama, K. Mizoguchi, H. Honda, K. Kume, R. Matsushita and T. Matsuyama: Synth. Met. **57** (1993) 4962.
78) R. J. Elliott: Phys. Rev. **96** (1954) 266.
79) Y. Nogami, J.-P. Pouget and T. Ishiguro: Synth. Met. **62** (1994) 257.
80) M. J. Winokur, P. Wamsley, J. Moulton, P. Smith and A. J. Heeger: Macromolecules **24** (1991) 3812.
81) G. Gustafsson, O. Inganäs, H. Österholm and J. Laakso: Polymer **32** (1991) 1574.
82) R. T. Schumacher and C. P. Slichter: Phys. Rev. **101** (1956) 58.
83) N. S. Sariciftci, A. Grupp and M. Mehring: Chem. Phys. Lett. **192** (1992) 375.
84) M. Schaerli, H. Kiess, G. Harbeke, W. Berlinger, K. W. Blazey and K. A. Mueller: *Electronic Properties of Conjugated Polymers*, eds. H. Kuzmany, M. Mehring and S. Roth (Springer-Verlag, Berlin, 1987) Springer Series in Solid State Science, Vol. 76, p. 277.
85) S. Masubuchi, S. Kazama, R. Matsushita and T. Matsuyama: submitted to Synth. Met.
86) M. Weger: J. Phys. (Paris) **39** (1978) C6–1456.
87) F. Beuneu and P. Monod: Phys. Rev. B **18** (1978) 2422.
88) K. Mizoguchi, K. Misoo, K. Kume, K. Kaneto, T. Shiraishi and K. Yoshino: Synth. Met. **18** (1989) 195 and references therein.
89) Recently, a similar conclusion was reported for K^+-doped polyacetylene by M. Nechtschein and Y. W. Park: *Proc. Int. Conf. Science and Technology of Synthetic Metals (ICSM'94), Seoul, 1994*, to be published in Synth. Met.
90) K. Mizoguchi, F. Shimizu, K. Kume and S. Masubuchi: Synth. Met. **41** (1991) 185.
91) F. Shimizu, K. Mizoguchi, S. Masubuchi and K. Kume: Synth. Met. **55** (1993) 720.
92) S. Masubuchi: unpublished data.
93) F. Devreux, F. Genoud, M. Nechtschein, J. P. Travers and G. Bidan: J. Phys. (Paris) **44** (1983) C3–621.
94) K. Mizoguchi: unpublished data.
95) See, for a recent interpretation, N. S. Sariciftci, A. J. Heeger and Y. Cao: Phys. Rev. B **49** (1994) 5988.
96) K. Kume, K. Mizuno, K. Mizoguchi, K. Nomura, H. Takayama, S. Ishihara, J. Tanaka, M. Tanaka, H. Fujimoto and H. Shirakawa: J. Phys. (Paris) **44** (1983) C3–353.
97) M. Kletter, A. G. MacDiarmid, A. J. Heeger, E. Faulques, S. Lefrant, P. Bernier, F. Barbarin, J. P. Blanc, J. P. Germain and H. Robert: Mol. Cryst. Liq. Cryst. **83** (1982) 165.
98) S. Kivelson and A. J. Heeger: Synth. Met. **22** (1988) 371.
99) S. Masubuchi, S. Kazama, K. Mizoguchi, F. Shimizu, K. Kume, R. Matsushita and T. Matsuyama: in preparation for publication.